Actin-based deformations of the nucleus control multiciliated ependymal cell differentiation.

Marianne Basso[1]#, Alexia Mahuzier[1]#, Ana-Maria Lennon-Duménil[2], Marion Faucourt[1], Alice Meunier[1], Nathalie Spassky[1], Nathalie Delgehyr[1*].

[1] Cilia biology and neurogenesis team, Institut de biologie de l'Ecole normale supérieure (IBENS),Ecole normale supérieure, CNRS, INSERM, PSL Research University, 75005, Paris, France.

[2] Institut Curie, INSERM U932, PSL Research University, 75005 Paris, France.

# Contributed equally.

*Corresponding author: delgehyr@bio.ens.psl.eu

ABSTRACT

Ependymal cells (ECs) are multi-ciliated cells in the brain that contribute to cerebrospinal fluid flow. ECs are specified at embryonic stages but differentiate and grow cilia later in development. Differentiation depends on genes such as GEMC1 and MCIDAS with E2F4/5 but also on cell cycle related factors. In the mouse brain, we observe that nuclear deformation accompanies EC differentiation. Tampering with these deformations either by decreasing F-actin levels or by severing the link between the nucleus and the actin cytoskeleton blocks differentiation. Conversely, increasing F-actin by knocking out the Arp2/3 complex inhibitor Arpin activates differentiation. Thus, actin polymerization triggers nuclear deformation and jump-starts the signaling that produce differentiated ECs. We show evidence that one of the players in this process is the retinoblastoma 1 (RB1) protein whose phosphorylation prompts MCIDAS activation. Overall, this study reveals an important role for actin-based mechanical inputs to the nucleus as controlling factors in cell differentiation.

Key words: Multiciliated, Ependyma, Differentiation, Actin, Nucleus, Mechanotransduction, Cell Cycle, MCIDAS, Retinoblastoma

INTRODUCTION

Multiciliated Ependymal cells (ECs) are located along brain ventricles. They form a protective barrier to the brain parenchyma and contribute to the cerebrospinal fluid (CSF) flow through the beating of their motile cilia[1]. Impairment of this flow correlates with age-related dementia[2], schizophrenia[3] and hydrocephalus[4], diseases whose onset is not always understood.

In mammalian brain, lineage tracing experiments show that ECs are sister cells of the adult neural stem cell[5,6], deriving from embryonic progenitors[7] but acquiring their own identity at later stages.

Differentiation of muticiliated cells depends on Notch inhibition that is required for the activation of the master regulators GEMC1 followed by MCIDAS and other effectors[8]. Both GEMC1 and MCIDAS interact with E2F4 or 5 and DP1 to promote transcriptional control of multiciliated cell differentiation[9]. Cell cycle related factors, such as Cdk1 and 2, are also involved in the differentiation of these post-mitotic cells[10,11]. The cues that trigger the activation of the different factors required for differentiation are not clear.

Neural stem cell progenitors are sensitive to forces during their proliferative and differentiating stages in neurons or oligodendrocytes[12], and it is known in stem cells in general that forces can be directly transmitted to the nucleus through the cytoskeleton[13]. Key players in this transmission are the LINC complexes that span the nuclear envelope and link the nucleoskeleton to the cytoskeleton[14]. In these complexes, the inner nuclear membrane proteins, the Sun family, contact the lamina (nucleoskeleton) and interact with a specific domain (KASH domain) of the outer nuclear membrane proteins (the NESPRIN family). Nesprins interact with either microtubules, intermediate filaments or actin. Actin has been shown to contribute to nuclear morphology and positioning in different systems (e.g. migrating fibroblasts[15], oocytes[16]). Interestingly, mechanical forces experienced by the nucleus alter gene expression[17,18] and promote cell cycle events[19-22].

In this context, we sought to uncover the cues that drive EC differentiation. We observed a connection between actin accumulation, nuclear deformation and differentiation. Other results imply that RB1 is involved in transducing nuclear deformations to activate EC differentiation.

RESULTS

Nuclei deform during ependymal cell differentiation.

To decipher the mechanisms triggering ECs differentiation, we stained lateral ventricles of mice expressing centrin 2-GFP[23] during the process of differentiation (Post-natal day 5, P5) with Lamin-B1 antibodies. We observed a large diversity of shapes and localizations of nuclei (Fig.1A). The centrin2-GFP allows us to determine the stage of EC differentiation. Cells at the surface of the ventricle with two centrin dots are progenitors. Then a cloud or ring-like structures of centrin appear near the two centrin dots, indicating the formation of pro-centrioles around deuterosomes (differentiating cells). Finally, several dots (on average 50[24]) of centrin are released from the deuterosomes and migrate toward the plasma membrane (multi basal body cells) where they dock to form the basal bodies at the base of motile cilia[25]. In the tissue, nuclei are quite close to each other, sometimes in depth; it is thus challenging to associate each nucleus with the corresponding centrin staining. To quantify the change in nuclear morphology, we therefore electroporated centrin2-GFP expressing brains at the onset of differentiation (P1) with membrane-cherry (Mb-Cherry). This reporter stains the membranes of the electroporated cells allowing the identification of which nucleus goes with which apical surface, where

centrioles are located, to assess differentiation stages. On electroporated lateral walls stained for Lamin-B1, we noted that during the process of differentiation (P5) the nuclei gain in volume (1.7x increase between progenitor and multi-basal body stages, Fig. 1A-B), change shape (becoming 2x flatter at the poles, Fig. 1A, C) and migrate toward the plasma membrane (moving around 2 μm up on average, Fig 1A, D). Thus, nuclei are drastically changing during the process of ependymal differentiation.

Actin, but not microtubules, are involved in nuclear deformation and EC differentiation

Nuclear deformation and localization depend on the cell cytoskeleton[26,27]. F-actin and microtubule staining on lateral wall during EC differentiation show that both networks undergo massive rearrangement, accumulating near the centrioles during the first steps of differentiation (Fig.S1A-D). To explore the contribution of both F-actin and microtubules in the shape of nuclei, we treated explants of lateral walls containing cells in the process of differentiation (P5) with drugs leading to actin (cytochalasin D) or microtubule (nocodazole) depolymerization for 20 hours. We then fixed and stained the explants for Lamin-B1. Cytochalasin-D perturbed the morphology of the nuclei of differentiated cells while nocodazole had no effect (Fig.S1E). In keeping with this, interfering with the microtubule molecular motor dynein had no effect on either nuclear deformation (Fig. S2 A-C) or EC differentiation (Fig. S2 D-G).

Since microtubules appeared dispensable for nuclear deformation and EC differentiation, we focused in the following on the actin cytoskeleton. Different actin polymerization complexes contribute to the actin network in multiciliated cells[28]. To assess whether F-actin accumulation during differentiation depends on the Arp2/3 complex (branched F-actin) or on Formins (linear F-actin), we treated explants of lateral walls bearing differentiating ECs (P5) with inhibitors of the Arp2/3 complex (CK666) or of the Formins (SMIFH2) for 20h and then fixed and stained them with Phalloidin (FigS1F, G). Only the treatment with CK666 decreased the accumulation of F-actin in differentiating cells compared to surrounding progenitor cells, suggesting its contribution to actin accumulation. To perturb the branched F-actin polymerization *in vivo*, we electroporated at differentiation onset (P1) an shRNA against *Arp3* for which the sequence was validated[29]. ARP3 is part of the Arp2/3 complex that nucleates the branched F-actin cytoskeleton. We checked by performing phalloidin staining at P5 on electroporated lateral walls that the sh*Arp3* decreases F-actin accumulation in differentiating cells compared to control (Fig.S1H, I) and relatively to untransfected surrounding progenitor cells. Lamin-B1 staining in cells depleted for *Arp3* showed that the nuclei do not flatten as much as in control electroporated cells, and migrate less toward the apical side (Fig.2A-C), while nuclear volumes remain similar to control (data not shown).

To check the effect of *Arp3* depletion on EC differentiation, we stained lateral ventricles of centrin 2-GFP expressing mice, electroporated at P1 with the sh*Arp3* or a control plasmid and Mb-Cherry, during the process of differentiation (P5) and after it (P15). Already from P5, we observed that fewer progenitors differentiated compared to controls (Fig.2D, E). We should note that some of the electroporated cells might already have been engaged in the process of differentiation at the time of electroporation as differentiation is asynchronous, starting before the electroporation for some cells. This is consistent with the fact that at P15, we observed a much stronger defect in EC differentiation in cells electroporated with the sh*Arp3* compared to the control (Fig.2F, G). All together this data suggests that branched F-actin is involved in the deformation / localization of the nuclei to promote EC differentiation.

If this were the case, we would expect that performing the inverse experiment, i.e. increasing actin polymerization, would increase nuclear deformation and EC differentiation. To test this hypothesis, we examined EC differentiation in an *Arpin* conditional KO mouse; the *Arpin* gene encodes for a negative regulator of the Arp2/3 complex so the knockout is expected to have enhanced branched actin polymerization[30]. We electroporated at P1 the lateral ventricle of *Arpin* conditional KO mice with the Cre recombinase and the Mb-Cherry marker. We first confirmed that removing *Arpin* increases F-actin accumulation in differentiating ependymal cells compared to control electroporation and relative to untransfected surrounding progenitors (Fig.S1H, I). We also stained the electroporated lateral walls for Lamin-B1 and observed that increasing F-actin polymerization triggers nuclei deformation and migration toward the apical surface at earlier stages than control cells (Fig.3A-C).

Finally, we also assessed whether increasing F-actin during the differentiation perturbs EC differentiation by staining for centriolar markers. We observed that removing *Arpin* at the differentiation onset led to an increase in differentiated cells (Fig.3D, E) at P5. Similarly, at P15 we observed significantly more ECs in the animal electroporated with Cre compared to the control (Fig.3F, G). These results suggest that premature increase of Arp2/3 activity led to a premature differentiation of progenitors in ependymal cells.

Severing the link between the nucleus and the cytoskeleton perturbs nuclear deformation and ependymal differentiation.

F-actin has many functions in cells so decreasing or increasing actin amounts could have off-target effects. To address this issue, we left the actin intact, but perturbed its link to the nucleus by expressing in the cells at the onset of differentiation (P1) a dominant negative construct composed of the KASH domain from NESPRIN1[31]. This domain displaces the endogenous NESPRINS by interacting with the SUN proteins, but cannot interact with the cytoskeleton. As an alternative, we also performed

an shRNA against *Syne2* (encoding for NESPRIN2) that is expressed during the differentiation (Fig.S3A, B), using a validated sequence[32] that decreased NESPRIN2 (Fig.S3C, D).

We first assessed whether the perturbation of the LINC complex changed the F-actin organization during ependymal differentiation. We stained with Phalloidin at P5, lateral ventricles electroporated at P1 with either the KASH domain or the sh*Syne2* or a control plasmid and Mb-Cherry. In both cases (KASH expression or sh*Syne2*), we did not observe changes in the F-actin organization compared to the control electroporated cells (Fig.S3E, F) and relative to untransfected surrounding progenitor cells.

We also stained for Lamin-B1 and observed that the nuclei of differentiating cells (P5) expressing the KASH or depleted for *Syne2* flatten less than control nuclei and remain in the depth of the tissue (Fig.4A-C and Fig.S4A-C).

Thus, removing the LINC complex is sufficient to perturb nuclear morphology without affecting F-actin polymerization. We then assessed how the cells are differentiating in absence of a functional LINC complex. At P5, when the cells are differentiating, expressing the KASH domain already slightly impairs differentiation (Fig.4D, E). At P15, the effect on ependymal differentiation is more clearly visible in cells expressing the KASH-domain as well as in cells depleted for *Syne2* (Fig.4F, G and Fig.S4D, E). All together, these experiments show that severing the LINC between the nucleus and the cytoskeleton is sufficient to perturb the nuclear morphology and EC differentiation without affecting the actin cytoskeleton. We conclude that nuclear deformation and EC differentiation go hand-in-hand, with nuclear deformation seemingly triggering EC differentiation.

S-phase transition factors are downstream of nuclear deformations during EC differentiation

This result begs the question as to what is transducing the mechanical deformation of the nucleus to the transcription factors that are known to control the differentiation of multiciliated cells. Interestingly, mechanical strain or cell confinement triggers cell cycle events and notably the transition between G1 and S phases[19-21]. Multiciliated cell differentiation depends on cell cycle related factors such as CDK2 and 1[10,11], even if the cells are post-mitotic, as well as on the master regulators GEMC1 and MCIDAS that together with E2F4 or 5 activate transcription of specific genes [9]. In cycling cells, CDK2 is known to phosphorylate retinoblastoma protein (RB1), triggering the release of E2F transcription factors from their interaction with RB1 and allowing them to activate S-phase specific genes to transition out of G1[33]. In ependymal cells, we know from previous work that CDK2 is required for the early steps of multiciliated differentiation[11,34] and that RB1 is hyperphosphorylated in differentiating EC[34].

To assess whether these phosphorylation events are driving differentiation, we expressed a non-phosphorylable version of RB1 (hRB1ΔCDK), where all the phospho-sites have been mutated in

Alanine[35], together with the reporter Mb-Cherry from differentiation onset (P1) and analyzed the resulting differentiation at P15. We observed that the cells expressing hRB1ΔCDK differentiate less than the control cells (Fig.5A, B), suggesting that the phosphorylation of RB1 is required for ependymal differentiation. We next wondered whether MCIDAS function relies on RB1 phosphorylation. To check this, we electroporated control plasmids or a plasmid coding for MCIDAS or both a plasmid coding for MCIDAS and a plasmid coding for the non-phosphorylable RB1 (tagged with an IRES-GFP) at P1. We fixed and stained the electroporated lateral wall a few days later (P3) to assess the early step of differentiation. We observed that while MCIDAS overexpression is able to induce a rapid ependymal differentiation, this capacity is impaired in cells expressing non-phosphorylable RB1 (Fig.5C, D). Thus, RB1 phosphorylation is needed for MCIDAS to perform its function.

If nuclear deformation is upstream of RB1 phosphorylation and E2F release, then forcing RB1 phosphorylation or removing it (the outcome of phosphorylation) in absence of nuclear deformation (such as in cell depleted for *Arp3*, Fig.2) should trigger ependymal differentiation. We thus used an shRNA against *Rb1*, previously validated[36] and that depleted phospho-RB1 in our system (Fig.S5A). We co-expressed a tagged version (IRES GFP) of the sh*Arp3* with this sh*Rb1* from differentiation onset and assessed the resulting effect on mature tissue (P15). As expected cells depleted for *Arp3* did not differentiate in ependymal cells. However, while depleting *Rb*1 alone as no specific effect (Fig.S5B, C), cells depleted for both *Arp3* and *Rb1* differentiated almost as good as the control cells (Fig.5E, F).Thus, mimicking the G1/ S transition (that is removing RB1) is sufficient to rescue ependymal differentiation in absence of nuclear deformations.

To assess whether changes in nuclear shape are linked to RB1 phosphorylation, we performed staining for Phospho-RB1 in cells of the lateral wall depleted of *Arp3* (from differentiation onset) that were shown to have impaired both nuclear deformation and ependymal differentiation (Fig.2). We observed that Phospho-RB1 failed to accumulate in the nucleus in cells depleted for *Arp3* compared to control (Fig.6A, B). Unphosphorylated RB1 is anchored by Lamin-A and LAP2α in the nucleoplasm[37-40]. This anchorage is important to protect RB1 from phosphorylation[41,42] and degradation[37]. On the other hand, Lamin-A is recruited at the nuclear membrane following mechanical strain on isolated nuclei[43] and increases with tissue stiffness, directing differentiation in other systems[44,45]. In this context, it is interesting to note that we observed an increase in Lamin-A contributed by an increase at the nuclear envelope (3x in average, Fig.6C, S5D), leading to a decrease of the ratio between nucleoplasmic and nuclear membrane bound Lamin-A (Fig.6C, D). This Lamin-A accumulation at the onset of EC differentiation, also coincides with the beginning of nucleoplasmic Lamin-A phosphorylation[10], as reported following nuclear deformation[42,46], a process important for its degradation[46]. A possibility, therefore, is that nuclear deformation leads to a recruitment of Lamin-A to the nuclear envelope, leading to an increase in RB1 accessibility in the nucleoplasm, and subsequently to its phosphorylation

and degradation. Thus, overexpressing Lamin-A in the nucleoplasm should block RB1 phosphorylation and EC differentiation. Interestingly, when we overexpressed a mCherry tagged version of Lamin-A, it localized similarly to the endogenous Lamin-A in the progenitors (ratio of mCherry-Lamin-A intensity in the nucleoplasm/ membrane bound of 0.4) but failed to be recruited to the nuclear envelope following initiation of EC differentiation (Fig.6C, D). Accordingly, cells overexpressing this mainly nucleoplasmic mCherry-Lamin-A from differentiation onset (electroporation at P1 with Mb-Cherry) failed to properly phosphorylate RB1 (Fig.6A, B) and did not differentiate properly (Fig6E, F). To assess whether the effect of Lamin-A overexpression on EC differentiation depends on RB1 being protected from phosphorylation/ degradation, we co-electroporated mCherry-Lamin-A and the shRNA against *Rb1* and analyzed the EC differentiation (Fig.6 E, F). In these conditions, we observed that removing RB1 is sufficient to restore EC differentiation in presence of nucleoplasmic mCherry-Lamin-A.

Thus, RB1 phosphorylation is a likely process for activating the differentiation in response to actin accumulation, nuclear deformation and Lamin-A re-localization.

DISCUSSION

Impairing nuclear deformation either by decreasing actin (sh*Arp3*, Fig.2) or by severing the link between the nucleus and the actin without affecting actin polymerization (KASH expression or sh*Syne2* Fig.4, S3-4), impairs EC differentiation. Conversely, forcing nuclear deformation by increasing actin polymerization (*Arpin*$^{KO/lox}$; Cre) accelerates differentiation (Fig.3). Our results thus show that mechanical constraints on the nucleus are important for EC differentiation in the mouse brain. Accordingly, to this nuclear stress on ependymal progenitors, Lamin-A at the nuclear envelope (Fig.6C, S5D) and DNA-damage increase[34,47].

We also show that RB1 is important for ependymal differentiation and that its removal rescue the absence of nuclear deformation (Fig.5). Furthermore, we posit that RB1 and its interaction with Lamin-A provide a possible explanation for how nuclear deformation impacts transcription factor activity for differentiation (Fig.5, 6). Intriguingly, both GEMC1 and MCIDAS interact with E2F proteins (4 and 5 respectively) and MCIDAS overexpression induces differentiation only if RB1 is phosphorylated (Fig.5C, D). Thus, nuclear deformation induces RB1 phosphorylation that will allow the release of E2F present in the cells and the activation of the multiciliated master regulators. Cells will remain in undifferentiated state until the nucleus is constrained by the actin cytoskeleton. This constraint will then induce the first steps of cell cycle-like activation that will trigger ependymal differentiation without inducing DNA replication[34].

The mechanical cues leading to actin accumulation that will act on the nucleus are not known. Neural stem cell progenitors are submitted to a variety of forces ranging from tissue growth (not

accounted by division[7]), changes in morphology (going from elongated to more cuboidal during differentiation) and pressure or shear stress generated by the cerebrospinal fluid[12,48]. Interestingly, stretch activated channels, like PIEZO1 are involved in neural stem cell differentiation[49] and may contribute to some aspect of multiciliated cell differentiation[50].

MATERIALs AND METHODS

Transgenic mice

All animal studies were performed in accordance with the guidelines of the European Community and French Ministry of Agriculture and were approved by the Ethic comity Charles Darwin (C2EA-05) and "Direction départementale de la protection des populations de Paris", (Approval number Ce5/2012/107; APAFiS #9343). Most of the mouse strains have already been described: wild-type are RjOrl:SWISS (Janvier labs), Cen2–GFP [23] (B6D2-Tg(CAG-EGFP/CETN2)3-4Jgg/J, The Jackson Laboratory); Arpin conditional knockout mice (Arpin^{lox}) were generated at CIPHE (Centre d'Immunophénomique, Marseille, France) using CRISPR cas-9 technology.

Plasmids

We cloned the shRNA sequences in the shRNA backbone vectors pcDNA-U6-shRNA and pTRIP-U6-shRNA-IRES-PGK-GFP-WPRE as previously described[51]. The control shRNA (shCtrl) was generated from AllStars Negative Control siRNA (Qiagen), which does not recognize mammalian RNAs. The reporter plasmid encoding membrane Cherry (Mb-Cherry) under the control of the CAGGS promoter was co-transfected with pcDNA-U6-shRNA and was a gift from Xavier Morin. All cells expressing the shRNA-GFP (pTRIP-U6-shRNA-IRES-PGK-GFP-WPRE) or cells expressing pCAGGS-mCherry (Mb-Cherry), which were co-transfected with the untagged pcDNA-U6-shRNA, were considered to be depleted.

shRNA sequences were validated in referenced paper and in this study: shArp3[29]: TTAGCTCTCTTCTACATCTGC (Fig.S1H, I); shSyne2[32]: AGCCACAGAACTCCAAAAT (Fig.S3C, D); shRb1[36]: AGTTAGGACTGTTATGAAT (Fig.S5C).

The pCAGGS-Cre plasmid is gift from X. Morin. The KASH domain construct is a gift from A. Merdes[32] and is tagged with GFP. The p150Glued-CC1 domain construct is a gift from NJ Quintyne[52] and is tagged with dsRed. The pCMV HA hRB1 delta CDK was a gift from S.Dowdy (Addgene plasmid # 58906 ; http://n2t.net/addgene:58906 ; RRID:Addgene_58906)[35]. HA hRB1 delta CDK was subcloned at BamHI restriction site on pIRES2-EGFP vector (Clontech). The Mcidas-GFP construct was a gift from S Taraviras,

in our hand the GFP was barely detectable. pCMV-tdTomato is from Clontech. mCherry-LaminA-C-18 was a gift from M. Davidson (Addgene plasmid #55068).

Postnatal electroporation

Electroporation was performed on one-day-old pups as previously described[53]. shRNA in the U6 backbone (untagged) (2.5μg) were co-transfected with the reporter plasmid Mb-Cherry or with plasmids encoding shRNA in the pTRIP backbone (IRES GFP) (1.5μg). MCIDAS-GFP (2μg) was electroporated either with pTRIP-shNeg or with HA hRB1 delta CDK-IRES2GFP (2μg). Cherry-LmnA (1.5μg) was electroporated either with pcDNA-U6-shNeg (2μg) or pcDNA-U6-shRb1 (2μg). All cells expressing the reporter were assumed to express both the reporter and the plasmid of interest.

Immunostaining

Lateral walls of the lateral brain ventricles were dissected, fixed, and immunostained as previously described[54]. The same area (rostro-dorsal) of the lateral walls was used throughout the study. The tissue was treated with 0.1% triton in BRB80 (80 mM K-Pipes pH6.8; 1 mM MgCl2; 1 mM Na-EGTA) for 1 min and fixed in methanol at −20°C for 10 min, most of the time. For phalloidin stained tissues, they were detergent-treated and then fixed in 4% PFA in BRB80 for 8 min, for phospho-RB1 staining or tissue electroporated with an IRES-GFP containing construct, the tissue were fixed in 4% PFA in BRB80. The following antibodies were used:

rabbit or rat anti-dsRed (1:200, Clontech 632496 or 5F8 1:400, Chromotek 5f8-100); chicken anti-GFP (1:800, Aves GFP-1020); mouse IgG2b anti-FOP (FGFR10P, 1:500, Abnova H00011116-MO), mouse IgG1 anti-beta-catenin (1:1000, Millipore05-665), mouse IgG2b anti-Sas6 (1:700, Santa-Cruz Sc-81431), mouse IgG1 anti-LaminB1 (1:1000, Sant-Cruz Sc-374015), lapin anti-Deup1 (1:2000) [55], Lapin anti-phospho-RB (Cell Signaling 8516), rabbit anti-Nesprin2 (1/100, gift from Greg Gundersen[56]), rat anti-tubulin YL1/2 (1:100, Sigma), mouse IgG2a anti-centrin (20H5 1:1000, Merck) and species-specific Alexa Fluor secondary antibodies (1:800, Invitrogen). Phalloidin-A488 or A568 were used at a dilution of 1:50 with primary and secondary antibodies.

Microscopy

<u>Optical imagery</u>

Images (230-nm z-steps) of fixed samples were obtained with an inverted LSM 880 Airyscan Zeiss with 63x 1.4NA oil-immersion objectives on confocal mode, except for the Phalloidin staining were it was used in the airyscan mode (180nm z-steps), and Zen2 software. Z-stack projections are shown. Only the 7 most apical plans are shown for phalloidin staining. For P150-CC1 and KASH nuclei some intermediate Z were removed to allow visualisation of the transfected nuclei in the depth of the tissue. The KASH-GFP or the Cherry-LmnA around the nucleus are not visible on images representative of EC

differentiation as the Z-stack including the apical surface does not include the whole nuclei deeper in the tissue.

Drug treatments

Lateral wall explants were immersed for the indicated times at 37°C with 5% CO_2 in DMEM-Glutamax (Invitrogen) supplemented with 10% FCS, 1% penicillin/streptomycin and cytochalasin-D (2μM, Sigma) to depolymerise actin, SMIFH2 (60μM, Sigma) to inhibit formin[57], CK666 (100μM, Sigma) to inhibit the Arp2/3 complex or Nocodazole (10μM, Sigma) to depolymerize microtubules. The lateral ventricular wall of the opposite side of each mouse brain were used as control and immersed in the same media containing an amount of DMSO equivalent to that of the drug.

Cell cultures

Differentiating ependymal cells were cultured as previously described[54].

In vitro transfection:

We transfected 10ng of the plasmid of interest with 10ng of reporter (pCMV-tdTomato) on $0.2x10^6$ cells in suspension (before D0) with 0.04μl of Jetprime (Polyplus) according to manufacturer protocol. The cells were seeded onto a drop of 20μl on a coverslip. 500μl of DMEM-Glutamax complemented with 10% FBS and 1% PS was added after 30minutes of incubation. Media was changed to DMEM-Glutamax 1% PS without serum the day after (D0). Cells were fixed and analyzed 7 days after serum starvation (D7). Cells expressing the reporter were considered as co-transfected.

3D modelling

Imaris 9.8.0 software was used for 3D modelling.

Data analysis

All analyses were performed on images of the rostro-dorsal part of the lateral walls of the lateral ventricles to maximize reproducibility.

<u>Measurement of phalloidin or YL1/2 fluorescence intensity</u>

Total mean actin (phalloidin fluorescence) or Tyr-tubulin (YL1/2 staining) intensity of fluorescence within cell borders were measured with ImageJ software on the sum projection of the 7 most apical z-stack sections of the cells. Quantification was normalised with respect to the mean signal intensity in the three closest non-transfected progenitor cells or the mean intensity of progenitor cells of the same image. The results are expressed as the ratio of the values of the cells over the mean values of the progenitor cells.

<u>Characterisation of nuclear shape</u>

Nuclei of cells co-transfected with Mb-Cherry were acquired for their Lamin-B1 staining. Analysis were performed with the Imaris software. For *in vivo* samples, a first loose manual segmentation was performed to exclude nuclei of the untransfected cells. This step was not required for cell in culture.

Then an automatic segmentation was performed using Surface and 0.2 grain size resolution. The volume is a quantification of how much space the Surface object occupies (Imaris reference manual). To obtain the pole to pole elongation index, the nucleus is fitted to an ellipse, the dimension of the three principal axes (a, b, c) of the best-fitted ellipsoid into the surface, the moments of inertia along the axes of ellipsoid are computed and optimized to match the moment of inertia of the surface. The ellipsoid has homogeneous mass distribution within the surface object. The pole to pole elongation index is the ellipsoid prolate; define as $e_{prolate}= (2a^2/a^2+b^2)*(1-((a^2+b^2)/2c^2))$ (Imaris reference manual). The centrin or FOP staining were segmented using dot and 0.25 μm size. The distance of the nucleus to the surface was calculated as the difference in z position of the highest centriole (anchored to the plasma membrane with primary or motile cilia) and the centre of the nucleus. Centre and not the highest part of the nucleus were taken in account, as they are more representative of the nucleus position in a very crowded environment.

Characterisation of cell differentiation stages

Only transfected cells with an apical contact at the surface of the ventricle were taken in account. When cells were stained with FOP or Centrin2-GFP, progenitors were considered to have only 2 dots, differentiating cells unresolved or donut like structures, multiciliated cells several resolved dots.

Centrin2-GFP might resolved earlier differentiating cells than FOP (not shown).

Sas6 or Deup1 staining, respectively pro-centrioles or deuterosomes, were used to confirm the differentiating cells when possible with the antibodies combinations and fixations.

To increase reproducibility, we counted the stages of the cells surrounding the transfected cells. At P15, images with 60 to 80% (average 65.8%±1.7sem) multiciliated cells were taken in account. At P5, images with 60 to 70% (average 65.6% ±0.4sem) progenitors cells were taken in account.

Measurement of NESPRIN2 levels:

Total mean of NESPRIN2 intensity of fluorescence were measured with ImageJ software in differentiating ependymal cells in vitro on maximum projection of the cell nuclei. Segmentations of the nuclei were performed using automatic thresholding with a triangle filter on Hoechst staining. Background taken in three independent zones in the images were subtracted from the mean value of NESPRIN2 levels for all measurment. The quantification was normalised with respect to the mean signal intensity in the non-transfected progenitor cells or the mean intensity of progenitor cells of the same image. The results are expressed as the ratio of the values of the cells over the mean values of the progenitor cells.

Measurement of phospho-RB1 staining:

Total mean of phospho-RB1 intensity of fluorescence were measured with ImageJ software in differentiating ependymal cells at P5 transfected with MbCherry, on the sum projection of the 5 most central z-stack sections of the nucleus normalised with respect to the mean signal intensity in the three

closest non-transfected progenitor cells. The results are expressed as the ratio of the values of the transfected cells over the mean values of the three surrounding control cells.

Measurement of Lamin-AC staining:

Total mean of Lamin-AC intensity of fluorescence were measured with ImageJ software in differentiating ependymal cells at P5 transfected with MbCherry or not, on the most central z-stack sections of the nucleus. Nuclear membrane intensity was determined by doing a line along the nuclear membrane, nucleoplasmic staining intensity was determined where the nuclear membrane was not doing circonvolutions. The results are expressed as the ratio of the values of the nucleoplasm and of the nuclear membrane or the results were normalised with respect to the mean signal intensity in progenitor cells of individual experiments.

Statistics

Means of two conditions were compared with the Mann-Whitney test. Means of more than two conditions were analysed by one-way ANOVA followed by Dunn's multiple comparison tests (GraphPad Prism 6.0). Analysis of cell distribution at different stages were performed by two-way ANOVA with Sidak's multiple comparisons test. Scatter plots are presented as the mean±sem. ROUT methods were used to remove outliers generated by phalloidin and NESPRIN2 quantification, with a Q value of 1% (GraphPad Prism 6.0). All results were obtained in at least three independent experiments on at least three different animals or cell cultures.

ACKNOWLEDGEMENTS

The data that support the findings of this study are available within the Article and Supplementary Files, or available from the authors upon request. We are grateful to J. Gleeson for providing the centrin2-GFP mice. We thank X. Morin for the CAAGS-mb-Cherry and CAAGS-Cre plasmids, I. Caillé and S. Scotto for the shRNA backbones, A. Merdes for the KASH plasmid, S. Dowdy for the hRB1ΔCDK plasmid. G. Gundersen for the NESPRIN2 antibody. S. Taraviras for the Mcidas plasmid. NJ Quintyne for the p150-CC1 plasmid. M. Davidson for the mCherry-LaminA-C-18 plasmid. We are grateful to A. Delecourt, E. Touzalin, G. Firmin and L. Le Moal for their help with the animal husbandry. We thanks M. Bornens for all his input over the year. We are grateful to all members of the Spassky laboratory as well as to J. Plastino for comments and discussion.

The team was funded by the Agence Nationale de la Recherche Investissements d'Avenir (ANR-10-LABX-54MEMO LIFE and ANR-11-IDEX-0001-02 PSL* Research University). The Spassky team is supported by the Inserm, the CNRS, the ENS, the ANR (ANR-20-CE45-0019, ANR-21-CE16-0016, and ANR-22-CE16-0011), the Fondation pour la Recherche Médicale (FRMEQU202103012767), the

Fondation Pierre-Gilles de Gennes (FPGG03) and the European Research Council (ERCConsolidatorgrant 647466).

REFERENCES

1. Kyrousi, C., Lygerou, Z., and Taraviras, S. (2017). How a radial glial cell decides to become a multiciliated ependymal cell. Glia *65*, 1032-1042. https://doi.org/10.1002/glia.23118.
2. Rubenstein, E. (1998). Relationship of senescence of cerebrospinal fluid circulatory system to dementias of the aged. The Lancet *351*, 283-285. http://dx.doi.org/10.1016/S0140-6736(97)09234-9.
3. Eom, T.-Y., Han, S.B., Kim, J., Blundon, J.A., Wang, Y.-D., Yu, J., Anderson, K., Kaminski, D.B., Sakurada, S.M., Pruett-Miller, S.M., et al. (2020). Schizophrenia-related microdeletion causes defective ciliary motility and brain ventricle enlargement via microRNA-dependent mechanisms in mice. Nature Communications *11*, 912. 10.1038/s41467-020-14628-y.
4. Zhang, J., Williams, M.A., and Rigamonti, D. (2006). Genetics of human hydrocephalus. J Neurol *253*, 1255-1266. 10.1007/s00415-006-0245-5.
5. Ortiz-Alvarez, G., Daclin, M., Shihavuddin, A., Lansade, P., Fortoul, A., Faucourt, M., Clavreul, S., Lalioti, M.E., Taraviras, S., Hippenmeyer, S., et al. (2019). Adult Neural Stem Cells and Multiciliated Ependymal Cells Share a Common Lineage Regulated by the Geminin Family Members. Neuron *102*, 159-172 e157. 10.1016/j.neuron.2019.01.051.
6. Redmond, S.A., Figueres-Oñate, M., Obernier, K., Nascimento, M.A., Parraguez, J.I., López-Mascaraque, L., Fuentealba, L.C., and Alvarez-Buylla, A. (2019). Development of Ependymal and Postnatal Neural Stem Cells and Their Origin from a Common Embryonic Progenitor. Cell Reports *27*, 429-441.e423. https://doi.org/10.1016/j.celrep.2019.01.088.
7. Spassky, N., Merkle, F.T., Flames, N., Tramontin, A.D., Garcia-Verdugo, J.M., and Alvarez-Buylla, A. (2005). Adult ependymal cells are postmitotic and are derived from radial glial cells during embryogenesis. J Neurosci *25*, 10-18.
8. Boutin, C., and Kodjabachian, L. (2019). Biology of multiciliated cells. Curr Opin Genet Dev *56*, 1-7. 10.1016/j.gde.2019.04.006.
9. Lewis, M., and Stracker, T.H. (2021). Transcriptional regulation of multiciliated cell differentiation. Seminars in Cell & Developmental Biology *110*, 51-60. https://doi.org/10.1016/j.semcdb.2020.04.007.
10. Al Jord, A., Shihavuddin, A., Servignat d'Aout, R., Faucourt, M., Genovesio, A., Karaiskou, A., Sobczak-Thepot, J., Spassky, N., and Meunier, A. (2017). Calibrated mitotic oscillator drives motile ciliogenesis. Science *358*, 803-806. 10.1126/science.aan8311.
11. Vladar, E.K., Stratton, M.B., Saal, M.L., Salazar-De Simone, G., Wang, X., Wolgemuth, D., Stearns, T., and Axelrod, J.D. (2018). Cyclin-dependent kinase control of motile ciliogenesis. Elife *7*. 10.7554/eLife.36375.
12. Abuwarda, H., and Pathak, M.M. (2020). Mechanobiology of neural development. Current Opinion in Cell Biology *66*, 104-111. https://doi.org/10.1016/j.ceb.2020.05.012.
13. Heo, S.-J., Cosgrove, B.D., Dai, E.N., and Mauck, R.L. (2018). Mechano-adaptation of the stem cell nucleus. Nucleus *9*, 9-19. 10.1080/19491034.2017.1371398.
14. Alam, S., Lovett, D.B., Dickinson, R.B., Roux, K.J., and Lele, T.P. (2014). Chapter Eight - Nuclear Forces and Cell Mechanosensing. In Progress in Molecular Biology and Translational Science, A.J. Engler, and S. Kumar, eds. (Academic Press), pp. 205-215. https://doi.org/10.1016/B978-0-12-394624-9.00008-7.
15. Zhu, R., Liu, C., and Gundersen, G.G. (2018). Nuclear positioning in migrating fibroblasts. Seminars in Cell & Developmental Biology *82*, 41-50. https://doi.org/10.1016/j.semcdb.2017.11.006.

16. Almonacid, M., Ahmed, W.W., Bussonnier, M., Mailly, P., Betz, T., Voituriez, R., Gov, N.S., and Verlhac, M.-H. (2015). Active diffusion positions the nucleus in mouse oocytes. Nature Cell Biology *17*, 470-479. 10.1038/ncb3131.
17. Uhler, C., and Shivashankar, G.V. (2017). Regulation of genome organization and gene expression by nuclear mechanotransduction. Nature Reviews Molecular Cell Biology *18*, 717. 10.1038/nrm.2017.101.
18. Wang, N., Tytell, J.D., and Ingber, D.E. (2009). Mechanotransduction at a distance: mechanically coupling the extracellular matrix with the nucleus. Nature Reviews Molecular Cell Biology *10*, 75-82. 10.1038/nrm2594.
19. Aureille, J., Buffière-Ribot, V., Harvey, B.E., Boyault, C., Pernet, L., Andersen, T., Bacola, G., Balland, M., Fraboulet, S., Van Landeghem, L., and Guilluy, C. (2019). Nuclear envelope deformation controls cell cycle progression in response to mechanical force. EMBO reports *20*, e48084. 10.15252/embr.201948084.
20. Benham-Pyle, B.W., Pruitt, B.L., and Nelson, W.J. (2015). Cell adhesion. Mechanical strain induces E-cadherin-dependent Yap1 and β-catenin activation to drive cell cycle entry. Science *348*, 1024-1027. 10.1126/science.aaa4559.
21. Uroz, M., Wistorf, S., Serra-Picamal, X., Conte, V., Sales-Pardo, M., Roca-Cusachs, P., Guimerà, R., and Trepat, X. (2018). Regulation of cell cycle progression by cell–cell and cell–matrix forces. Nature Cell Biology *20*, 646-654. 10.1038/s41556-018-0107-2.
22. Dantas, M., Oliveira, A., Aguiar, P., Maiato, H., and Ferreira, J.G. (2022). Nuclear tension controls mitotic entry by regulating cyclin B1 nuclear translocation. Journal of Cell Biology *221*. 10.1083/jcb.202205051.
23. Higginbotham, H., Bielas, S., Tanaka, T., and Gleeson, J.G. (2004). Transgenic mouse line with green-fluorescent protein-labeled Centrin 2 allows visualization of the centrosome in living cells. Transgenic Res *13*, 155-164.
24. Mahuzier, A., Shihavuddin, A., Fournier, C., Lansade, P., Faucourt, M., Menezes, N., Meunier, A., Garfa-Traoré, M., Carlier, M.-F., Voituriez, R., et al. (2018). Ependymal cilia beating induces an actin network to protect centrioles against shear stress. Nature Communications *9*, 2279. 10.1038/s41467-018-04676-w.
25. Al Jord, A., Lemaitre, A.I., Delgehyr, N., Faucourt, M., Spassky, N., and Meunier, A. (2014). Centriole amplification by mother and daughter centrioles differs in multiciliated cells. Nature *516*, 104-107.
26. Makhija, E., Jokhun, D.S., and Shivashankar, G.V. (2016). Nuclear deformability and telomere dynamics are regulated by cell geometric constraints. Proceedings of the National Academy of Sciences of the United States of America *113*, E32-E40. 10.1073/pnas.1513189113.
27. Ramdas, N.M., and Shivashankar, G.V. (2015). Cytoskeletal Control of Nuclear Morphology and Chromatin Organization. Journal of Molecular Biology *427*, 695-706. https://doi.org/10.1016/j.jmb.2014.09.008.
28. Hoffman, H.K., and Prekeris, R. (2022). Roles of the actin cytoskeleton in ciliogenesis. Journal of Cell Science *135*, jcs259030. 10.1242/jcs.259030.
29. Drummond, M.L., Li, M., Tarapore, E., Nguyen, T.T.L., Barouni, B.J., Cruz, S., Tan, K.C., Oro, A.E., and Atwood, S.X. (2018). Actin polymerization controls cilia-mediated signaling. Journal of Cell Biology *217*, 3255-3266. 10.1083/jcb.201703196.
30. Dang, I., Gorelik, R., Sousa-Blin, C., Derivery, E., Guérin, C., Linkner, J., Nemethova, M., Dumortier, J.G., Giger, F.A., Chipysheva, T.A., et al. (2013). Inhibitory signalling to the Arp2/3 complex steers cell migration. Nature *503*, 281-284. 10.1038/nature12611.
31. Starr, D.A., and Han, M. (2002). Role of ANC-1 in Tethering Nuclei to the Actin Cytoskeleton. Science *298*, 406-409. doi:10.1126/science.1075119.
32. Espigat-Georger, A., Dyachuk, V., Chemin, C., Emorine, L., and Merdes, A. (2016). Nuclear alignment in myotubes requires centrosome proteins recruited by nesprin-1. Journal of Cell Science *129*, 4227-4237. 10.1242/jcs.191767.

33. Rubin, S.M., Sage, J., and Skotheim, J.M. (2020). Integrating Old and New Paradigms of G1/S Control. Molecular Cell *80*, 183-192. https://doi.org/10.1016/j.molcel.2020.08.020.
34. Ortiz-Álvarez, G., Fortoul, A., Srivastava, A., Moreau, M.X., Bouloudi, B., Mailhes-Hamon, C., Delgehyr, N., Faucourt, M., Bahin, M., Blugeon, C., et al. (2022). p53/p21 pathway activation contributes to the ependymal fate decision downstream of GemC1. Cell Reports *41*, 111810. https://doi.org/10.1016/j.celrep.2022.111810.
35. Narasimha, A.M., Kaulich, M., Shapiro, G.S., Choi, Y.J., Sicinski, P., and Dowdy, S.F. (2014). Cyclin D activates the Rb tumor suppressor by mono-phosphorylation. eLife *3*, e02872. 10.7554/eLife.02872.
36. Taura, M., Suico, M.A., Koyama, K., Komatsu, K., Miyakita, R., Matsumoto, C., Kudo, E., Kariya, R., Goto, H., Kitajima, S., et al. (2012). Rb/E2F1 Regulates the Innate Immune Receptor Toll-Like Receptor 3 in Epithelial Cells. Molecular and Cellular Biology *32*, 1581-1590. doi:10.1128/MCB.06454-11.
37. Johnson, B.R., Nitta, R.T., Frock, R.L., Mounkes, L., Barbie, D.A., Stewart, C.L., Harlow, E., and Kennedy, B.K. (2004). A-type lamins regulate retinoblastoma protein function by promoting subnuclear localization and preventing proteasomal degradation. Proceedings of the National Academy of Sciences of the United States of America *101*, 9677-9682. 10.1073/pnas.0403250101.
38. Mancini, M.A., Shan, B., Nickerson, J.A., Penman, S., and Lee, W.H. (1994). The retinoblastoma gene product is a cell cycle-dependent, nuclear matrix-associated protein. Proceedings of the National Academy of Sciences *91*, 418-422. 10.1073/pnas.91.1.418.
39. Markiewicz, E., Dechat, T., Foisner, R., Quinlan, R.A., Hutchison, C.J., and Lippincott-Schwartz, J. (2002). Lamin A/C Binding Protein LAP2α Is Required for Nuclear Anchorage of Retinoblastoma Protein. Molecular Biology of the Cell *13*, 4401-4413. 10.1091/mbc.e02-07-0450.
40. Mittnacht, S., and Weinberg, R.A. (1991). G1/S phosphorylation of the retinoblastoma protein is associated with an altered affinity for the nuclear compartment. Cell *65*, 381-393. https://doi.org/10.1016/0092-8674(91)90456-9.
41. Dechat, T., Shimi, T., Adam, S.A., Rusinol, A.E., Andres, D.A., Spielmann, H.P., Sinensky, M.S., and Goldman, R.D. (2007). Alterations in mitosis and cell cycle progression caused by a mutant lamin A known to accelerate human aging. Proc Natl Acad Sci U S A *104*, 4955-4960. 10.1073/pnas.0700854104.
42. Van Berlo, J.H., Voncken, J.W., Kubben, N., Broers, J.L., Duisters, R., van Leeuwen, R.E., Crijns, H.J., Ramaekers, F.C., Hutchison, C.J., and Pinto, Y.M. (2005). A-type lamins are essential for TGF-beta1 induced PP2A to dephosphorylate transcription factors. Hum Mol Genet *14*, 2839-2849. 10.1093/hmg/ddi316.
43. Guilluy, C., Osborne, L.D., Van Landeghem, L., Sharek, L., Superfine, R., Garcia-Mata, R., and Burridge, K. (2014). Isolated nuclei adapt to force and reveal a mechanotransduction pathway in the nucleus. Nat Cell Biol *16*, 376-381. 10.1038/ncb2927.
44. Engler, A.J., Sen, S., Sweeney, H.L., and Discher, D.E. (2006). Matrix Elasticity Directs Stem Cell Lineage Specification. Cell *126*, 677-689. https://doi.org/10.1016/j.cell.2006.06.044.
45. Swift, J., Ivanovska, I.L., Buxboim, A., Harada, T., Dingal, P.C.D.P., Pinter, J., Pajerowski, J.D., Spinler, K.R., Shin, J.-W., Tewari, M., et al. (2013). Nuclear Lamin-A Scales with Tissue Stiffness and Enhances Matrix-Directed Differentiation. Science *341*, 1240104. 10.1126/science.1240104.
46. Buxboim, A., Swift, J., Irianto, J., Spinler, K.R., Dingal, P.C., Athirasala, A., Kao, Y.R., Cho, S., Harada, T., Shin, J.W., and Discher, D.E. (2014). Matrix elasticity regulates lamin-A,C phosphorylation and turnover with feedback to actomyosin. Curr Biol *24*, 1909-1917. 10.1016/j.cub.2014.07.001.
47. Cho, S., Vashisth, M., Abbas, A., Majkut, S., Vogel, K., Xia, Y., Ivanovska, I.L., Irianto, J., Tewari, M., Zhu, K., et al. (2019). Mechanosensing by the Lamina Protects against Nuclear Rupture,

DNA Damage, and Cell-Cycle Arrest. Dev Cell *49*, 920-935 e925. 10.1016/j.devcel.2019.04.020.
48. Desmond, M.E., and Jacobson, A.G. (1977). Embryonic brain enlargement requires cerebrospinal fluid pressure. Developmental Biology *57*, 188-198. https://doi.org/10.1016/0012-1606(77)90364-5.
49. Pathak, M.M., Nourse, J.L., Tran, T., Hwe, J., Arulmoli, J., Le, D.T., Bernardis, E., Flanagan, L.A., and Tombola, F. (2014). Stretch-activated ion channel Piezo1 directs lineage choice in human neural stem cells. Proc Natl Acad Sci U S A *111*, 16148-16153. 10.1073/pnas.1409802111.
50. Kulkarni, S., Marquez, J., Date, P., Ventrella, R., Mitchell, B.J., and Khokha, M.K. (2021). Mechanical stretch scales centriole number to apical area via Piezo1 in multiciliated cells. eLife *10*, e66076. 10.7554/eLife.66076.
51. Scotto-Lomassese, S., Nissant, A., Mota, T., Néant-Féry, M., Oostra, B.A., Greer, C.A., Lledo, P.-M., Trembleau, A., and Caillé, I. (2011). Fragile X Mental Retardation Protein Regulates New Neuron Differentiation in the Adult Olfactory Bulb. The Journal of Neuroscience *31*, 2205-2215. 10.1523/jneurosci.5514-10.2011.
52. Quintyne, N.J., Gill, S.R., Eckley, D.M., Crego, C.L., Compton, D.A., and Schroer, T.A. (1999). Dynactin Is Required for Microtubule Anchoring at Centrosomes. The Journal of Cell Biology *147*, 321-334. 10.1083/jcb.147.2.321.
53. Boutin, C., Diestel, S., Desoeuvre, A., Tiveron, M.C., and Cremer, H. (2008). Efficient in vivo electroporation of the postnatal rodent forebrain. PLoS One *3*, e1883.
54. Delgehyr, N., Meunier, A., Faucourt, M., Bosch Grau, M., Strehl, L., Janke, C., and Spassky, N. (2015). Chapter 2 - Ependymal cell differentiation, from monociliated to multiciliated cells. In Methods in Cell Biology, B. Renata, and F.M. Wallace, eds. (Academic Press), pp. 19-35. http://dx.doi.org/10.1016/bs.mcb.2015.01.004.
55. Mercey, O., Levine, M.S., LoMastro, G.M., Rostaing, P., Brotslaw, E., Gomez, V., Kumar, A., Spassky, N., Mitchell, B.J., Meunier, A., and Holland, A.J. (2019). Massive centriole production can occur in the absence of deuterosomes in multiciliated cells. Nat Cell Biol *21*, 1544-1552. 10.1038/s41556-019-0427-x.
56. Luxton, G.W.G., Gomes, E.R., Folker, E.S., Vintinner, E., and Gundersen, G.G. (2010). Linear Arrays of Nuclear Envelope Proteins Harness Retrograde Actin Flow for Nuclear Movement. Science *329*, 956-959. 10.1126/science.1189072.
57. Rizvi, S.A., Neidt, E.M., Cui, J., Feiger, Z., Skau, C.T., Gardel, M.L., Kozmin, S.A., and Kovar, D.R. (2009). Identification and characterization of a small molecule inhibitor of formin-mediated actin assembly. Chem Biol *16*, 1158-1168. 10.1016/j.chembiol.2009.10.006.

FIGURE LEGENDS

Figure 1: Nuclei deform during ependymal differentiation

A) Staining of Lamin-B1 (nuclear lamina, Grey) and Centrin2-GFP (centrioles, Green) during ependymal cell differentiation (postnatal day 5, P5) on whole mount lateral wall of centrin2-GFP mice. The different stages of differentiation are recognized according to the centrin2-GFP pattern: 2 dots = Progenitors, 2 dots + clouds or rings = differentiating cells, several dots (more than 5) = multi-basal bodies. Top view is a maximum projection of z-stacks. Side view is an Imaris 3D projection of the above cell (orange dashed circle) with segmented nuclei.

(B, D) Quantification of the nuclear shape during the different steps of ependymal differentiation at P5 on Imaris segmented nuclei of cells transfected at P1 with membrane-cherry (to be able to associate the nucleus to the differentiation stage). **B)** Volume **C)** Pole to pole elongation index (Prolate ellipticity)

D) Distance between the center of the nucleus and the highest centriole. Error bars represent the sem of n=54 progenitors, 66 differentiating and 54 multi-basal bodies cells from nine mice; p-values were determined by one-way ANOVA followed by Dunn's multiple comparison test; *** P≤0.001; ** P≤0.01. Scale bar = 5μm;

Figure 2: Decreasing ARP3 impairs nuclear reshaping and ependymal differentiation.

Wild-type **(A-C)** or Centrin2-GFP **(D, G)** mice transfected at P1 with mb-cherry as a reporter and either a control plasmid (Ctrl) or an shRNA against *Arp3* (sh*Arp3*).

A) Staining of Lamin-B1 (nuclear lamina, Grey) and FOP (centrioles, Green) during ependymal cell differentiation (P5) on whole mount lateral wall. Transfected cells, either control (top row) or sh*Arp3* (bottom row), are circled with orange dashed lines. Top view is a maximum projection of z-stacks. Side view is an Imaris 3D projection with segmented nuclei. The white dashed lines represent the plasma membrane.

(B, C) Quantification of nuclear shapes during the different steps of ependymal differentiation on Imaris segmented nuclei as in **A**. **B)** Pole to pole elongation index. **C)** Distance between the center of the nucleus and the highest centriole. Error bars represent the sem of n=26/ 73 progenitors, 36/ 29 differentiating and 29/ 39 multi-basal bodies transfected cells (Ctrl/ sh*Arp3*) from four mice; p-values from Mann-Whitney test; *** P≤0.001; ** P≤0.01; ns, P>0.05.

D) Staining of Centrin2-GFP (centrioles, Green), Sas6 (procentrioles, White), mb-cherry (reporter, Red) and beta-catenin (junction, Blue) during ependymal cell differentiation (P5) on whole mount lateral wall.

E) Quantification of the percentage of transfected cells as in **D** at each stage of differentiation at P5 (Prog=progenitors, Diff=Differentiating, Multi=multi-basal bodies). Error bars represent the sem of 5 experiments n=174 (Ctrl) and 183 (sh*Arp3*) transfected cells; p-values from two-way ANOVA followed by Sidak's multiple comparisons test; ** P≤0.01.

F) Staining of Centrin2-GFP (centrioles, Green), mb-cherry (reporter, Red) and beta-catenin (junction, Blue) in differentiated cells (P15) on whole mount lateral wall.

G) Quantification of the percentage of transfected cells as in **F** remaining as progenitors (Prog), still differentiating (Diff) or differentiated in ependymal cells (Multi), at P15. Error bars represent the sem of 4 or 3 experiments n=83 (Ctrl) and 93 (sh*Arp3*) transfected cells, respectively; p-values from two-way ANOVA followed by Sidak's multiple comparisons test; *** P≤0.001.

Scale bar = 5μm;

Figure 3: Increasing Arp2/3 complex activity facilitates nuclear reshaping and ependymal differentiation.

(A-G) Arpin$^{lox/lox}$ transfected at P1 with mb-cherry as a reporter and a control plasmid (Ctrl) or Arpin$^{KO/lox}$ mice transfected at P1 with mb-cherry as a reporter and a plasmid coding for the Cre recombinase (*Arpin*$^{KO/lox}$;Cre).

A) Staining of Lamin-B1 (nuclear lamina, Grey) and FOP (centrioles, Green) during ependymal cell differentiation (P5), on whole mount lateral wall. Transfected cells, either Ctrl (top row) or Arpin$^{KO/lox}$;Cre (bottom row) are circled with orange dashed lines. Top view is a maximum projection of z-stacks. Side view is an Imaris 3D projection with segmented nuclei. The white dashed lines represent the plasma membrane.

(B, C) Quantification of nuclear shapes during the different steps of ependymal differentiation on Imaris segmented nuclei of cells as in **A**. **B)** Pole to pole elongation index. **C)** Distance between the center of the nucleus and the highest centriole. Error bars represent the sem of n=48/ 53 progenitors, 50/ 31 differentiating and 40/ 40 multi-basal bodies cells (Ctrl/ *Arpin*$^{KO/lox}$;Cre) from 7 mice in Ctrl and 8 mice in *Arpin*$^{KO/lox}$;Cre; p-values from Mann-Whitney test; ** $P \leq 0.01$; * $p<0.05$; ns, $P>0.05$.

D) Staining of FOP (centrioles, Green), Deup1 (deuterosomes, White) and mb-cherry (reporter, Red) during ependymal cell differentiation (P5) on whole mount lateral wall.

E) Quantification of the percentage of transfected cells as in **D** at each stages of differentiation at P5. Error bars represent the sem of 5 (Ctrl) or 4 (*Arpin*$^{KO/lox}$;Cre) experiments, n=178 (Ctrl) and 145 (*Arpin*$^{KO/lox}$;Cre) transfected cells; Prog=progenitors, Diff=Differentiating and Multi=Multi-basal body cells. p-values from two-way ANOVA followed by Sidak's multiple comparisons test; *** $P \leq 0.001$; ns, $P>0.05$.

F) Staining of FOP (centrioles, Green) and mb-cherry (reporter, Red) in differentiated cells (P15) on whole mount lateral wall.

G) Quantification of the percentage of transfected cells as in **F** remaining as progenitors (Prog), still differentiating (Diff) or differentiated in ependymal cells (Multi) at P15. Error bars represent the sem of 6 (Ctrl) and 5 (*Arpin*$^{KO/lox}$;Cre) experiments, n=314 (Ctrl) and 151 (*Arpin*$^{KO/lox}$;Cre) transfected cells; p-values from two-way ANOVA followed by Sidak's multiple comparisons test; * $p=0.0416$.

Scale bar = 5μm;

Figure 4: Severing the link between the nucleus and the cytoskeleton impairs nuclear reshaping and ependymal differentiation.

Wild-type **(A-C)** or Centrin2-GFP **(D-G)** mice transfected at P1 with mb-cherry as a reporter and either a control plasmid (Ctrl) or the KASH-domain (dominant negative of the LINC complex, KASH).

A) Staining of Lamin-B1 (nuclear lamina, Grey) and FOP (centrioles, Green) during ependymal cell differentiation (P5) on whole mount lateral wall. Transfected cells, either Ctrl (top row) or KASH (bottom row), are circled with orange dashed lines. Top view is a maximum projection of z-stacks. Side view is an Imaris 3D projection with segmented nuclei. The white dashed lines represent the plasma membrane.

(B, C) Quantification of the nuclear shape during the different steps of ependymal differentiation on Imaris segmented nuclei as in **A**. **B)** Pole to pole elongation index. **C)** Distance between the center of the nucleus and the highest centriole. Error bars represent the sem of n=29/ 21 progenitors, 30/ 26 differentiating and 23/ 22 multi-basal bodies transfected cells (Ctrl/ KASH) from three mice; p-values from Mann-Whitney test * $P<0.05$; ns $P>0.05$; ** $P\leq0.01$.

D) Staining of Centrin2-GFP (centrioles, Green), Sas6 (procentrioles, white), mb-cherry (reporter, Red) and beta-catenin (junction, Blue) during ependymal cell differentiation (P5) on whole mount lateral wall.

E) Quantification of the percentage of transfected cells as in **D** at each stages of differentiation at P5. Error bars represent the sem of 5 experiments; n=131 (Ctrl) and 189 (KASH) transfected cells; Prog=Progenitor, Diff=Differentiating, Multi=multi-basal body cells. p-values from two-way ANOVA followed by Sidak's multiple comparisons test; ** $P\leq0.01$; * $P=0.035$; ns $P>0.05$.

F) Staining of Centrin2-GFP (centrioles, Green), mb-cherry (reporter, Red) and beta-catenin (junction, Blue) in differentiated cells (P15) on whole mount lateral wall.

G) Quantification of the percentage of transfected cells as in **F** remaining as progenitors (Prog), still differentiating (Diff) or differentiated (Multi) at P15. Error bars represent the sem of 6 (Ctrl) or 3 (KASH) experiments, n=148 (Ctrl) and 86 (KASH) transfected cells; p-values from two-way ANOVA followed by Sidak's multiple comparisons test; *** $P\leq0.001$.

Scale bar = 5μm;

Figure 5: RB1 is involved in ependymal differentiation following nuclear deformation.

A) Staining of centrin2-GFP (centrioles, Green), mb-cherry (reporter, Red) and beta-catenin (junctions, Blue) in differentiated cells (P15) on whole mount lateral wall of centrin2-GFP mice transfected at P1 with mb-cherry and either a control plasmid (Ctrl) or a plasmid coding for an unphosphorylable RB1 (hRB1-ΔCDK).

B) Quantification of the percentage of transfected cells as in **A** remaining as progenitors (Prog), still differentiating (Diff) or differentiated (Multi) at P15. Error bars represent the sem of 4 experiments, n=146 (Ctrl) and 148 (hRB1-ΔCDK) transfected cells; p-values from two-way ANOVA followed by Sidak's multiple comparisons test; *** $P\leq0.001$.

C) Staining of FOP (centrioles, Green), GFP (reporter, Red) and beta-catenin (junctions, Blue) in early differentiating cells (P3) on whole mount lateral wall of wild-type mice transfected at P1 with control plasmids (Ctrl= shNeg-IRES-GFP+ shNeg) or MCIDAS (shNeg-IRES-GFP+ MCIDAS) or both MCIDAS and unphosphorylatable RB1 (hRB1-ΔCDK -IRES-GFP+ MCIDAS).

D) Quantification of the percentage of transfected cells at P3 as in **C** in the different stages of differentiation: Progenitors (Prog), differentiating (Diff) or differentiated (Multi). Error bars represent the sem of 3 (Ctrl) or 8 (MCIDAS) or 5 (MCIDAS + hRB1-ΔCDK) experiments, n=75 (Ctrl), 198 (MCIDAS) and 123 (MCIDAS + hRB1-ΔCDK) transfected cells; p-values from two-way ANOVA followed by Sidak's multiple comparisons test; *** P≤0.0001; ** p≤0.01; * p≤0.05.

E) Staining of FOP (centrioles, Green), mb-cherry (reporter, Red) and beta-catenin (junction, Blue) in differentiated cells (P15) on whole mount lateral wall of wild-type mice transfected with a control plasmid (Ctrl= shNeg-IRES-GFP+ shNeg) or sh*Arp3 (shArp3*-IRES-GFP+ shNeg*)* or both sh*Arp3* and sh*Rb1 (shArp3*-IRES-GFP*+ shRb1)*. IRES containing constructs were used as reporter, less concentrated than the other plasmids (potentially explaining the decreased effect of sh*Arp3* compared to Fig.3).

F) Quantification of the percentage of transfected cells as in **E**, remaining as progenitors (Prog), still differentiating (Diff) or differentiated in ependymal cells (Multi), at P15. Error bars represent the sem of 6 (Ctrl) or 6 (sh*Arp3*) or 3 (sh*Arp3* + sh*Rb1*) experiments, n=109 (Ctrl), 155 (sh*Arp3*) and 68 (sh*Arp3*+ sh*Rb1*) transfected cells; p-values from two-way ANOVA followed by Sidak's multiple comparisons test; *** p≤0.001; for Prog Ctrl vs sh*Arp3*+ sh*Rb1* *p=0.0483; for Multi Ctrl vs sh*Arp3*+ sh*Rb1* *p=0.0151.

Scale bar = 5μm;

Figure 6: Nucleoplasmic Lamin-A impairs EC differentiation in a RB1 dependent manner.

A) Staining of phospho-RB1 (Green) and FOP (centrioles, Red) in differentiating cells transfected with mb-cherry (orange dashed circle) and either a control plasmid (Ctrl, top row) or an shRNA against *Arp3* (sh*Arp3*) or overexpressing Cherry-Lamin-A (OE LmnA).

B) Quantification of the fluorescence intensity of nuclear phospho-RB1 of transfected cells as in **A** normalized to the mean intensity of nuclear phospho-RB1 in three surrounding untransfected progenitors. Error bars represent the sem of n=19/ 16 /13 (Ctrl/ sh*Arp3/* OE LmnA) transfected cells. p-values from Mann-Whitney test. *** p≤0.001, * p=0.0125.

C) Top Row, staining of Lamin-A/C (Gray) and FOP (centrioles, Green) on whole mount lateral wall of wild-type mice at P5. Bottom row, staining of Cherry-LaminA (Cherry-LmnA, Gray) and Centrin2-GFP (centriole, Green) on whole mount lateral wall of centrin2-GFP mice at P5 electroporated at P1 with cherry-LmnA.

D) Quantification of the ratio of fluorescence intensity of Lamin-A/C (Ctrl) or Cherry-Lamin-A (OE LmnA) in the nucleoplasm over the one at the nuclear membrane. Error bars represent the sem of for progenitors of n=37/ 39; for differentiating of n=30/ 34 cells from 4/ 3 mice (Ctrl/ OE LmnA). p-values from two-way ANOVA followed by Sidak's multiple comparisons test; *** P≤0.001.

E) Staining of Centrin2-GFP (centrioles, Green), mb-cherry or Cherry-Lamina-A (Red) and beta-catenin (junction, Blue) in differentiated cells (P15) on whole mount lateral wall of Centrin2-GFP mice electroporated at P1 with mb-cherry and a control plasmid (Ctrl) or with Cherry-Lamin-A and shNeg (OE LmnA) or sh*Rb1 (*OE LmnA sh*Rb1)*.

F) Quantification of the percentage of transfected cells as in **E** remaining as progenitors (Prog), still differentiating (Diff) or differentiated (Multi) at P15. Error bars represent the sem of 4 (Ctrl) or 6 (Lamin-A + shNeg) and 5 (Lamin-A+ sh*Rb1*) experiments; n=88 (Ctrl), 141 (Lamin-A + shNeg) and 105 (Lamin-A + sh*Rb1*) transfected cells; p-values from two-way ANOVA followed by Sidak's multiple comparisons test; *** P≤0.001.

Scale bar = 5µm

Figure S1: Actin filaments polymerized by the Arp2/3 complex and microtubules accumulate during ependymal differentiation

All staining were performed on whole mount lateral wall during ependymal differentiation (post-natal day 5, P5). The different stages of differentiation are recognized according to centriole staining: 2 dots = Progenitors, 2 dots + clouds or rings = differentiating progenitors, several dots (more than 5) = multi-basal bodies.

A) Staining of F-actin (Phalloidin, Grey) and centrioles (FOP, Red).

B) Quantification of the F-actin fluorescence intensity on images as in **A** normalized to the mean fluorescence intensity of F-actin in progenitors. Error bars represent the sem of n=96 progenitors, 46 differentiating and 183 multi-basal bodies cells from four mice; p-values from one-way ANOVA followed by Dunn's multiple comparison test; *** P≤0.001.

C) Staining of Tyrosinated-Tubulin (YL1/2= polymerizing tubulin, Gray) and centrin (20H5= centrioles, Red).

D) Quantification of the Tyr-tubulin fluorescence intensity on images as in **C** normalized to the mean fluorescence intensity of Tyr-tubulin in progenitors. Error bars represent the sem of n=75 progenitors, 46 differentiating and 66 multi-basal body cells from three mice; p-values from one-way ANOVA followed by Dunn's multiple comparison test; *** P≤0.001.

E) Staining of lamin (Lamin-B1, Grey) and centrioles (FOP, Red) on explant treated with DMSO or nocodazole (microtubule inhibitor 10µM) or cytochalasin-D (F-actin inhibitor, 2µM) for 20h.

F) Staining of F-actin (Phalloidin, Grey) and centrioles (FOP, Red) on explant treated for 20h with DMSO or CK666 (100μM, Arp2/3 complex inhibitor) or SMIFH2 (60μM, formin inhibitor).

G) Quantification of the F-actin fluorescence intensity on differentiating ependymal cells on images as in **F** normalized to the mean fluorescence intensity of F-actin in progenitors of relative images. Error bars represent the sem of n=44, 46 and 50 differentiating cells treated with DMSO, CK666 or SMIFH2 respectively from four independent mice; p-values from one-way ANOVA followed by Dunn's multiple comparison test; *** P≤0.001.

H) Staining of F-actin (Phalloidin, Grey) and centrioles (FOP, Red) on cells transfected with mb-cherry (reporter, orange dashed line) and either a control plasmid (Ctrl) or an shRNA against *Arp3* (sh*Arp3*) or Arpin$^{KO/lox}$ mice electroporated with a plasmid encoding for the Cre recombinase.

I) Quantification of the F-actin fluorescence intensity on images as in **H** normalized to the mean fluorescence intensity of F-actin in untransfected progenitors of relative images. Error bars represent the sem of n=33, 25 and 20 transfected differentiating cells (Ctrl (wild type or Arpin$^{lox/lox}$ mice) or sh*Arp3* (wild-type mice) or Cre (Arpin$^{KO/lox}$ mice) respectively) from four mice; p-values from one-way ANOVA followed by Dunn's multiple comparison test; Ctrl vs sh*Arp3* **p=0.0076; Ctrl vs Arpin$^{KO/lox}$; Cre **p=0.0053. Scale bar = 5μm;

Figure S2: Disturbing Dynein does not affect ependymal differentiation.

Wild type **(A-C)** or Centrin2-GFP **(D-G)** mice transfected at P1 with mb-cherry as a reporter and either a control plasmid (Ctrl) or the p150-CC1 domain (dominant negative of dynein, p150-CC1).

A) Staining of Lamin-B1 (nuclear lamina, Grey) and FOP (centrioles, Green) during ependymal cell differentiation (P5) on whole mount lateral wall. Transfected cells, either Ctrl (top row) or p150-CC1 (bottom row), are circled with orange dashed lines. Top view is a maximum projection of z-stacks. Side view is an Imaris 3D projection with segmented nuclei. The white dashed lines represent the plasma membrane.

(B, C) Quantification of the nuclear shape during the different steps of ependymal differentiation on Imaris segmented nuclei as in **A**. **B)** Pole to pole elongation index. **C)** Distance between the center of the nucleus and the highest centriole. Error bars represent the sem of n=29/ 59 progenitors, 30/ 35 differentiating and 23/ 36 multi-basal bodies transfected cells (Ctrl/ p150-CC1) from three mice; p-values from Mann-Whitney test; ns, P>0.05. * p=0.0132. Control values are the same than on Figure 4.

D) Staining of Centrin2-GFP (centrioles, Green), Sas6 (procentrioles, White), mb-cherry (reporter, Red) and beta-catenin (junction, Blue) during ependymal cell differentiation (P5) on whole mount lateral wall.

E) Quantification of the percentage of transfected cells as in **D** at each stages of differentiation at P5. Error bars represent the sem of 5 experiments n=174 (Ctrl) and 175 (p150-CC1) transfected cells; p-

values from two-way ANOVA followed by Sidak's multiple comparisons test; ns, P>0.05. Control values are the same than on Figure 2 as the experiments were performed at the same time.

F) Staining of Centrin2-GFP (centrioles, Green), mb-cherry (reporter, Red) and beta-catenin (junction, Blue) in differentiated cells (P15) on whole mount lateral wall.

G) Quantification of the percentage of transfected cells as in **F** remaining as progenitors (Prog), still differentiating (Diff) or differentiated in ependymal cells (Multi) at P15. Error bars represent the sem of 4 (Ctrl) or 4 (p150-CC1) experiments n=83 (Ctrl) and 65 (p150-CC1) transfected cells; p-values from two-way ANOVA followed by Sidak's multiple comparisons test; *** P≤0.0001; ns, P>0.05. Control values are the same than on Figure 2.

Scale bar = 5µm;

Figure S3: NESPRIN2 localization and impact of LINC complex disruption on actin.

A) Staining of NESPRIN2 (LINC complex, White) on whole mount lateral wall at P5 (*in vivo*) or during ependymal cell differentiation *in vitro* (7 days after serum withdrawal D7) from Centrin2-GFP (centriole, Green) mice.

B) Quantification of the levels of intensity of NESPRIN2 staining at each stages of differentiation either progenitor (Prog), differentiating (Diff) or already differentiated (Multi) on *in vitro* culture as in **A**, normalized to the mean intensity of progenitor cells on each images. Error bars represent the sem of n=261 prog, 64 diff and 124 multi cells; from three independent cultures; p-values from Mann-Whitney test *** P≤0.0001; ns, P>0.05

C) Staining of NESPRIN2 (LINC complex, White) in differentiating cells on whole mount lateral wall at P5 electroporated at P1 (*in vivo*) or in progenitor cells at D7 transfected at D0 (*in vitro*)with either Ctrl or sh*Syne2* (depleted for NESPRIN2).

D) Quantification of the levels of intensity of NESPRIN2 staining *in vitro* in progenitor cells at D7 transfected with a control plasmid (Ctrl) or depleted for NESPRIN2 (sh*Syne2*) as in **B** normalized to the mean of intensity of untransfected progenitor cells on each images. Error bars represent the sem of n=30 cells; from three independent cultures; p-values from Mann-Whitney test *** P≤0.0001;

E) Staining of F-actin (Phalloidin, Grey) and centrioles (FOP, Red) at different stages of differentiation on whole mount lateral wall at P5 of wild-type mice transfected with mb-cherry (reporter, orange dashed line) and either a control plasmid (Ctrl) or the KASH-domain (KASH) or an shRNA against *Syne2* (sh*Syne2*).

F) Quantification of the F-actin fluorescence intensity on cells at different stages of differentiation on images as in **C** normalized to the mean fluorescence intensity of F-actin in untransfected progenitors of relative images. Error bars represent the sem of n=88/ 35/ 62 for progenitors, 33/ 14/ 30 for

differentiating and 58/ 21/ 19 for multi-basal body cells of Ctrl/ KASH/ sh*Syne2* respectively. No significant difference between the different conditions and Ctrl for a given stage as determined with the Mann-Whitney test.

Scale bar = 5μm;

Figure S4: Decreasing NESPRIN2 (a protein of the LINC complex) impairs nuclear re-shaping and ependymal differentiation.

Wild type **(A-C)** or Centrin2-GFP **(D-E)** mice transfected at P1 with mb-cherry as a reporter and either a control plasmid (Ctrl) or an shRNA against *Syne2* (sh*Syne2*).

A) Staining of Lamin-B1 (nuclear lamina, Grey) and FOP (centrioles, Green) during ependymal cell differentiation (P5) on whole mount lateral wall. Transfected cells, either Ctrl (top row) or sh*Syne2* (bottom row), are circled with orange dashed lines. Top view is a maximum projection of z-stacks. Side view is an Imaris 3D projection with segmented nuclei. The white dashed lines represent the plasma membrane.

(B, C) Quantification of the nuclear shape during the different steps of ependymal differentiation on Imaris segmented nuclei as in **A**. **B)** Pole to pole elongation index. **C)** Distance between the center of the nucleus and the highest centriole. Error bars represent the sem of n=26/ 37 progenitors, 36/ 15 differentiating and 29/ 30 multi-basal bodies transfected cells from four mice; p-values from Mann-Whitney test; ns, P>0.05;* p=0.041; *** P≤0.001. Control values are the same than on Figure 2.

D) Staining of Centrin2-GFP (centrioles, Green), mb-cherry (reporter, Red) and beta-catenin (junction, Blue) in differentiated cells (P15) on whole mount lateral wall.

E) Quantification of the percentage of transfected cells as in **D** differentiated in ependymal cells (Multi), still differentiating (Diff) or remaining as progenitors (Prog) at P15. Error bars represent the sem of 6 (Ctrl) or 3 (sh*Syne2*) experiments n=148 (Ctrl) and 84 (sh*Syne2*) transfected cells; p-values from two-way ANOVA followed by Sidak's multiple comparisons test; ** P=0.0034; ns. Control values are the same than on Figure 4.

Scale bar = 5μm;

Figure S5: sh*Rb1 in vivo*.

A) Staining of FOP (centrioles, Red) and phospho-RB1 (Green) during ependymal cell differentiation (P5) on whole mount lateral wall electroporated at P1 with mb-cherry and a control plasmid (Ctrl) or sh*Rb1* to assess depletion. Transfected cells are circled with orange dashed lines

B) Staining of centrin2-GFP (centrioles, Green), mb-cherry (reporter, Red) and beta-catenin (junctions, Blue) in differentiated cells (P15) on whole mount lateral wall of centrin2-GFP mice transfected at P1 with mb-cherry and either a control plasmid (Ctrl) or sh*Rb1*.

C) Quantification of the percentage of transfected cells as in **B**, either Control (ctrl) or sh*Rb1* remaining as progenitors (Prog), still differentiating (Diff) or differentiated in ependymal cells (Multi) at P15. Error bars represent the sem of 4 experiments n=146 (Ctrl same as in Figure 6D), 81 (shRb1) transfected cells; p-values from two-way ANOVA followed by Sidak's multiple comparisons test; ns, P>0.05.

D) Quantification of the fluorescence intensity of Lamin-A/C bound to the nuclear membrane at different stages of differentiation, normalized to the mean fluorescence intensity in progenitor cells. Error bars represent the sem of for progenitors of n=37; for differentiating of n=30, for multiciliated n=31 cells from 4 mice. p-values from two-way ANOVA followed by Sidak's multiple comparisons test; *** P≤0.001.

Scale bar = 5μm;

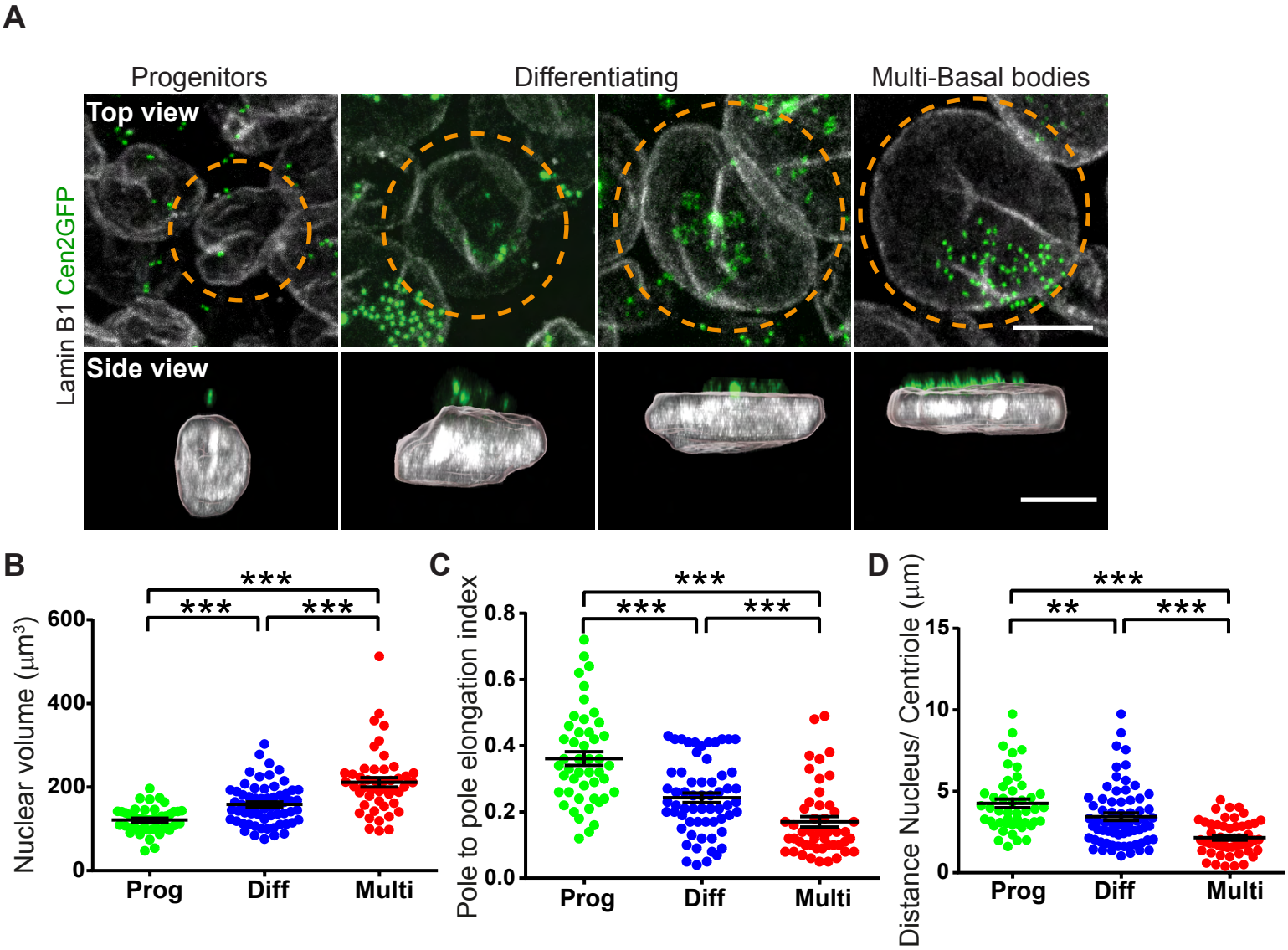
A
Progenitors
Differentiating
Multi-Basal bodies
Top view
Side view
Lamin B1 Cen2GFP
B
Nuclear volume (µm³)
600
400
200
0
***
***
***
Prog
Diff
Multi
C
Pole to pole elongation index
0.8
0.6
0.4
0.2
0.0
***
***
***
Prog
Diff
Multi
D
Distance Nucleus/ Centriole (µm)
15
10
5
0
***
**
***
Prog
Diff
Multi

Fig.1

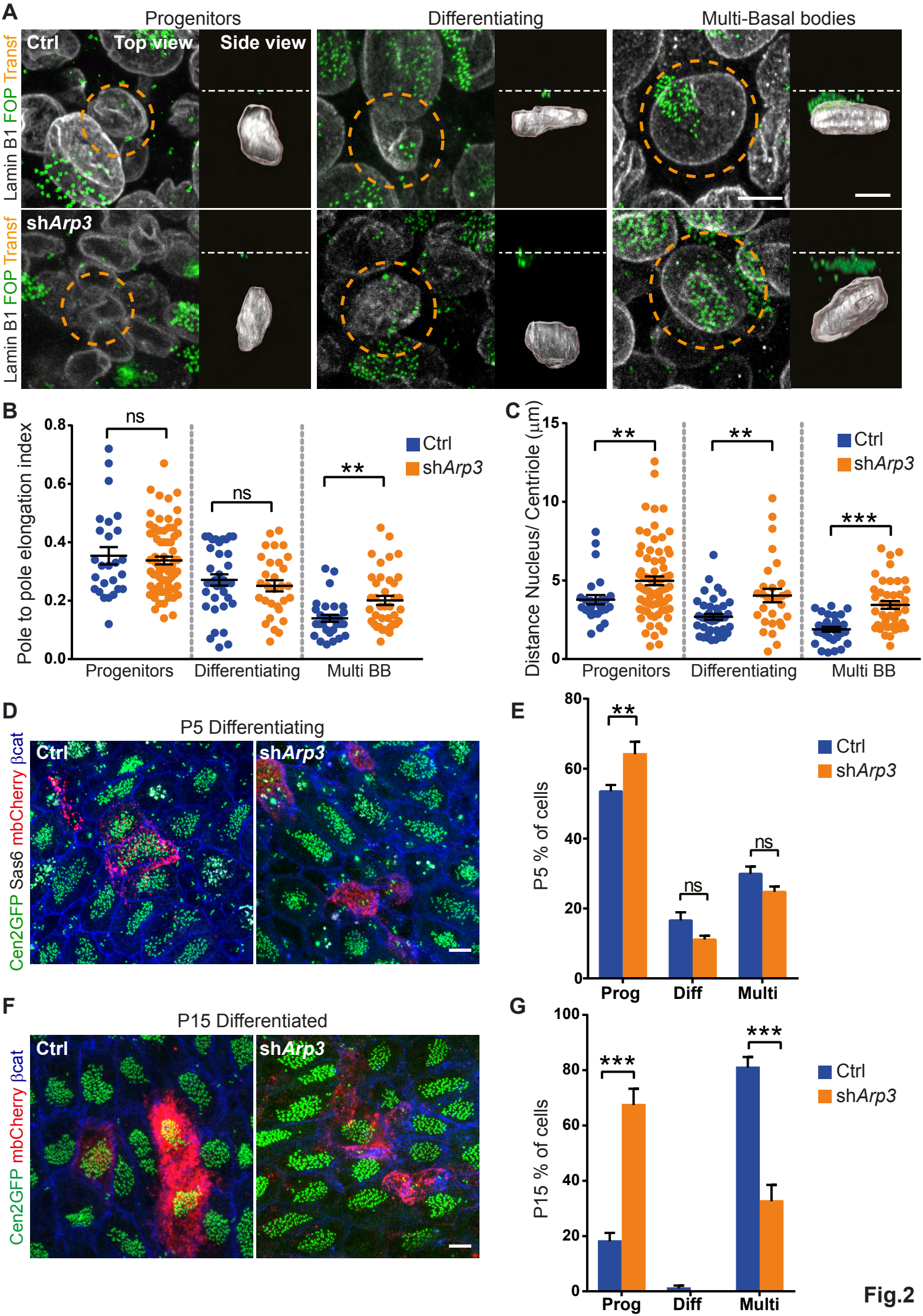
A
Progenitors
Differentiating
Multi-Basal bodies
Ctrl
Top view
Side view
shArp3
Lamin B1 FOP Transf
B
Pole to pole elongation index
ns
ns
**
Ctrl
shArp3
Progenitors
Differentiating
Multi BB
C
Distance Nucleus/ Centriole (µm)
**
**
***
Ctrl
shArp3
Progenitors
Differentiating
Multi BB
D
P5 Differentiating
Ctrl
shArp3
Cen2GFP Sas6 mbCherry βcat
E
P5 % of cells
**
ns
ns
Ctrl
shArp3
Prog
Diff
Multi
F
P15 Differentiated
Ctrl
shArp3
Cen2GFP mbCherry βcat
G
P15 % of cells
***
***
Ctrl
shArp3
Prog
Diff
Multi

Fig.2

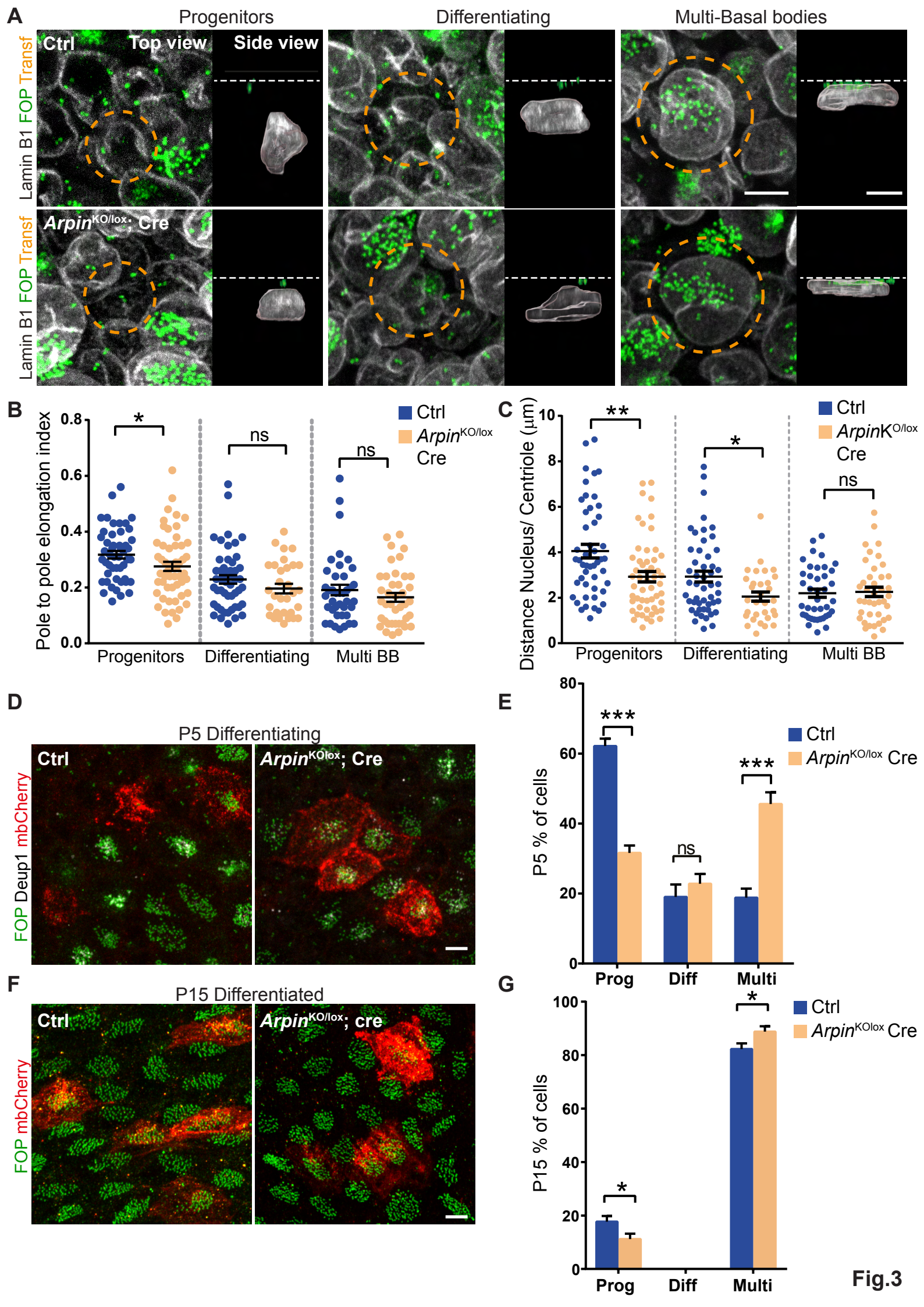
A
Progenitors
Differentiating
Multi-Basal bodies
Ctrl
Top view
Side view
Lamin B1 FOP Transf
Arpin KO/lox; Cre
B
Pole to pole elongation index
Ctrl
Arpin KO/lox Cre
Progenitors
Differentiating
Multi BB
ns
C
Distance Nucleus/ Centriole (µm)
D
P5 Differentiating
FOP Deup1 mbCherry
E
P5 % of cells
Prog
Diff
Multi
F
P15 Differentiated
FOP mbCherry
G
P15 % of cells
Fig.3

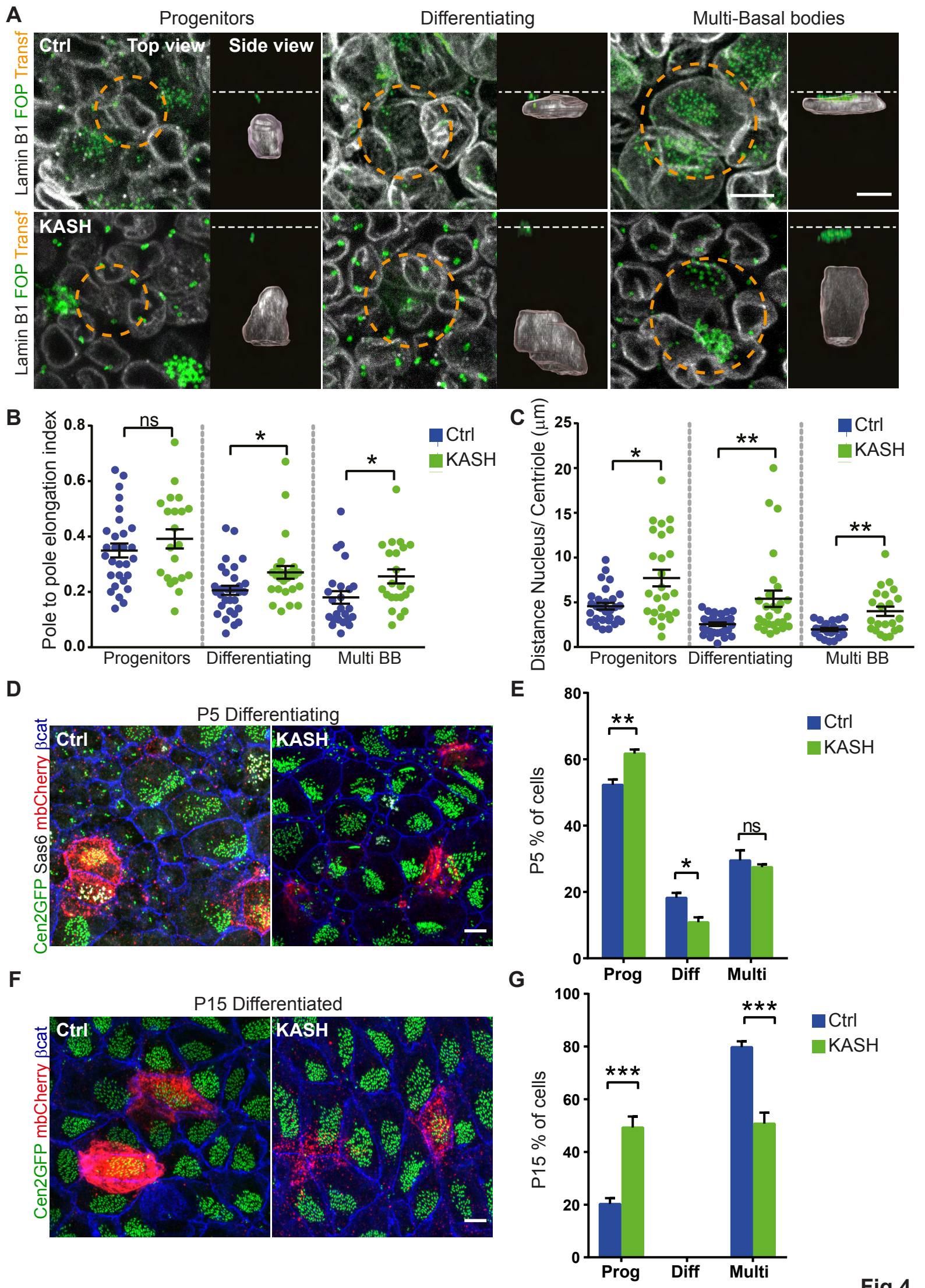
A
Progenitors
Differentiating
Multi-Basal bodies
Ctrl
Top view
Side view
KASH
Lamin B1 FOP Transf
B
Pole to pole elongation index
ns
*
*
Ctrl
KASH
Progenitors
Differentiating
Multi BB
C
Distance Nucleus/ Centriole (µm)
*
**
**
Ctrl
KASH
Progenitors
Differentiating
Multi BB
D
P5 Differentiating
Ctrl
KASH
Cen2GFP Sas6 mbCherry βcat
E
P5 % of cells
**
*
ns
Ctrl
KASH
Prog
Diff
Multi
F
P15 Differentiated
Ctrl
KASH
Cen2GFP mbCherry βcat
G
P15 % of cells
***
***
Ctrl
KASH
Prog
Diff
Multi

Fig.4

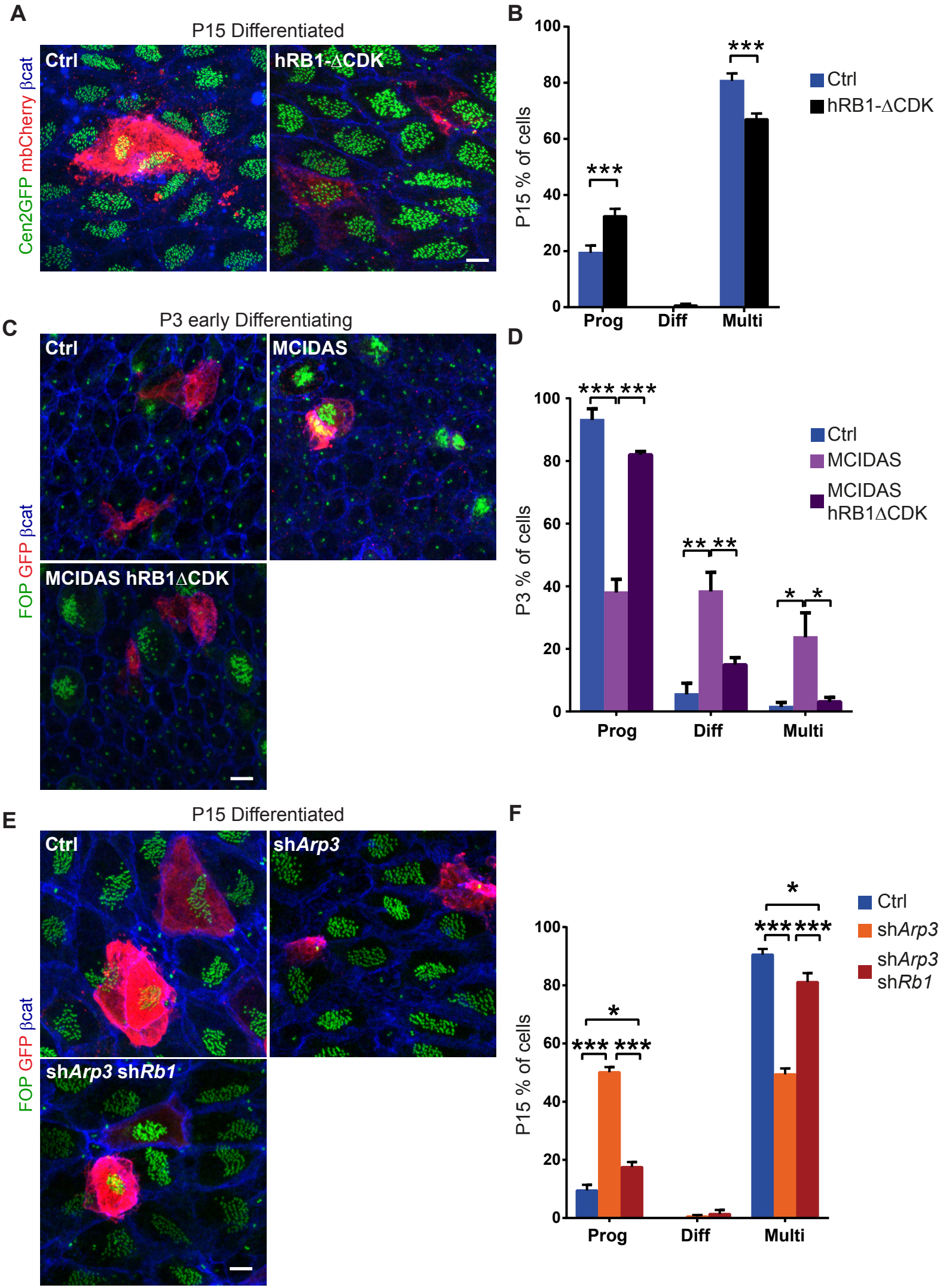
A
P15 Differentiated
Cen2GFP mbCherry βcat
Ctrl
hRB1-ΔCDK
B
P15 % of cells
100
80
60
40
20
0
***
***
Prog
Diff
Multi
Ctrl
hRB1-ΔCDK
C
P3 early Differentiating
FOP GFP βcat
Ctrl
MCIDAS
MCIDAS hRB1ΔCDK
D
P3 % of cells
*** ***
** **
* *
Prog
Diff
Multi
Ctrl
MCIDAS
MCIDAS hRB1ΔCDK
E
P15 Differentiated
FOP GFP βcat
Ctrl
shArp3
shArp3 shRb1
F
P15 % of cells
*
*** ***
*
*** ***
Prog
Diff
Multi
Ctrl
shArp3
shArp3 shRb1

Fig.5

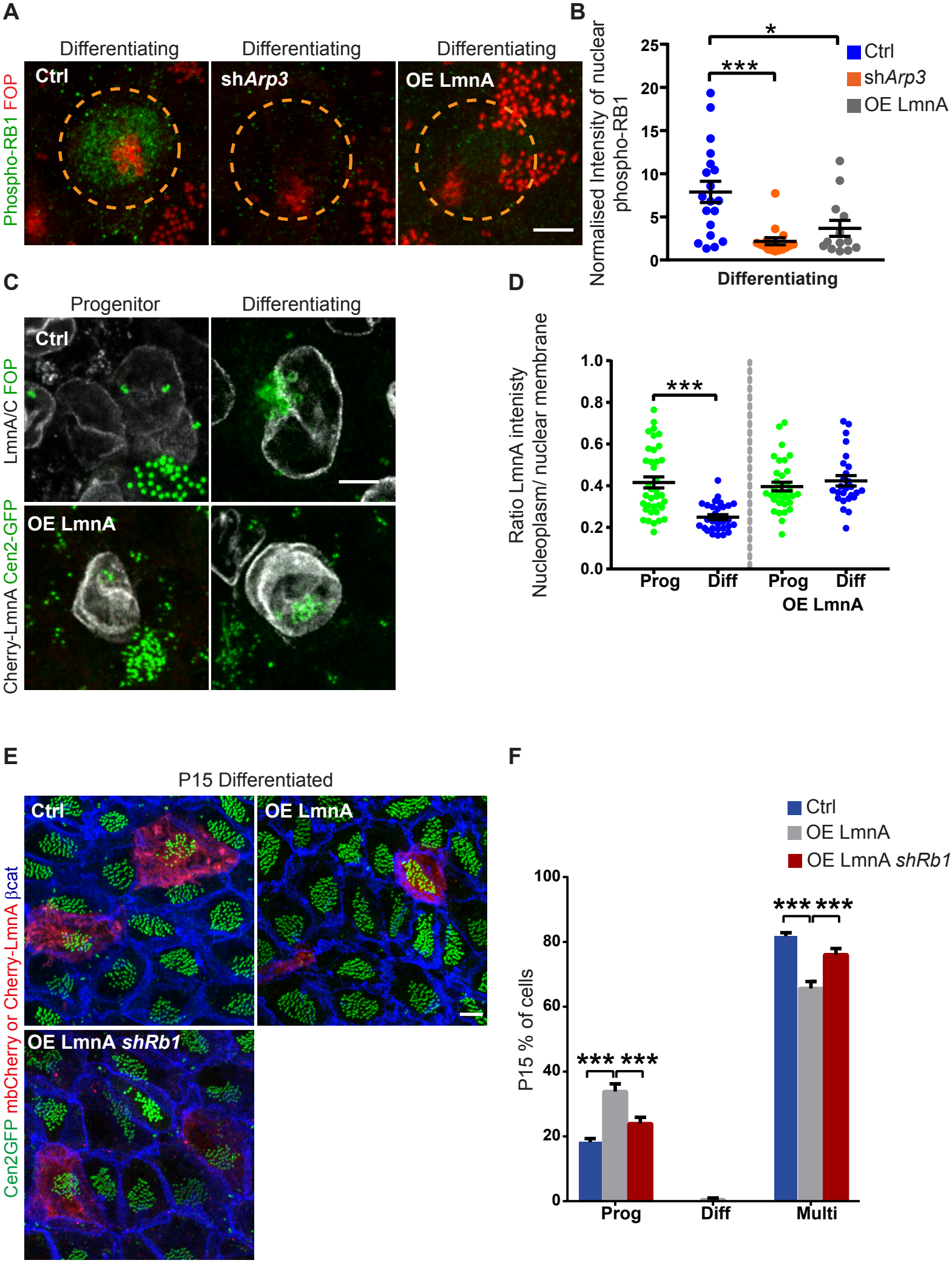
A
Differentiating
Differentiating
Differentiating
Ctrl
shArp3
OE LmnA
Phospho-RB1 FOP
B
Normalised Intensity of nuclear phospho-RB1
Differentiating
Ctrl
shArp3
OE LmnA
C
Progenitor
Differentiating
Ctrl
OE LmnA
LmnA/C FOP
Cherry-LmnA Cen2-GFP
D
Ratio LmnA intenisty Nucleoplasm/ nuclear membrane
Prog
Diff
Prog
Diff
OE LmnA
E
P15 Differentiated
Ctrl
OE LmnA
OE LmnA shRb1
Cen2GFP mbCherry or Cherry-LmnA βcat
F
Ctrl
OE LmnA
OE LmnA shRb1
P15 % of cells
Prog
Diff
Multi

Fig.6

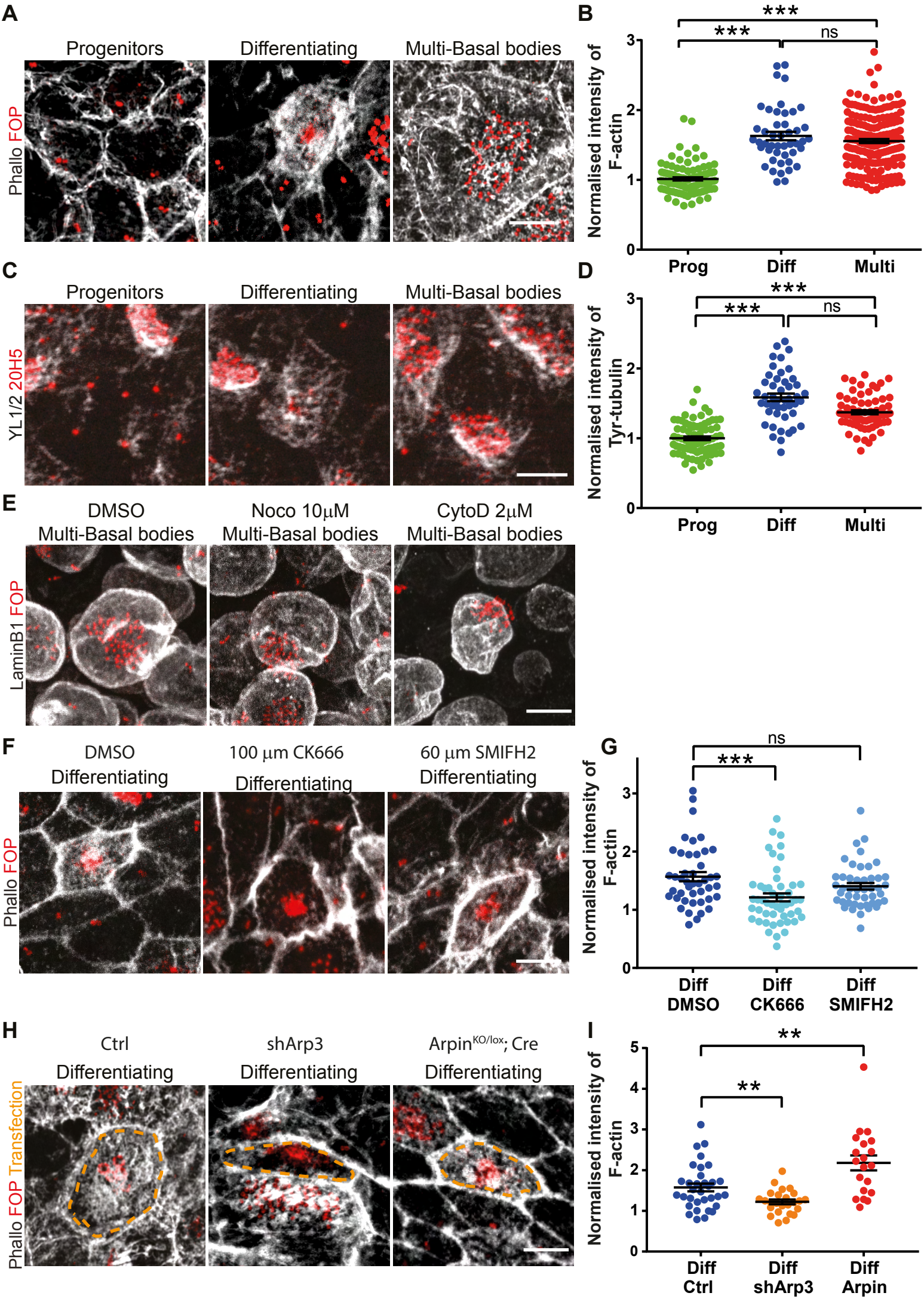
A
Progenitors
Differentiating
Multi-Basal bodies
Phallo FOP
B
***
***
ns
Normalised intensity of F-actin
Prog
Diff
Multi
C
Progenitors
Differentiating
Multi-Basal bodies
YL1/2 20H5
D
***
***
ns
Normalised intensity of Tyr-tubulin
Prog
Diff
Multi
E
DMSO
Multi-Basal bodies
Noco 10μM
Multi-Basal bodies
CytoD 2μM
Multi-Basal bodies
LaminB1 FOP
F
DMSO
Differentiating
100 μm CK666
Differentiating
60 μm SMIFH2
Differentiating
Phallo FOP
G
ns
***
Normalised intensity of F-actin
Diff DMSO
Diff CK666
Diff SMIFH2
H
Ctrl
Differentiating
shArp3
Differentiating
Arpin$^{KO/lox}$; Cre
Differentiating
Phallo FOP Transfection
I
**
**
Normalised intensity of F-actin
Diff Ctrl
Diff shArp3
Diff Arpin

Fig.S1

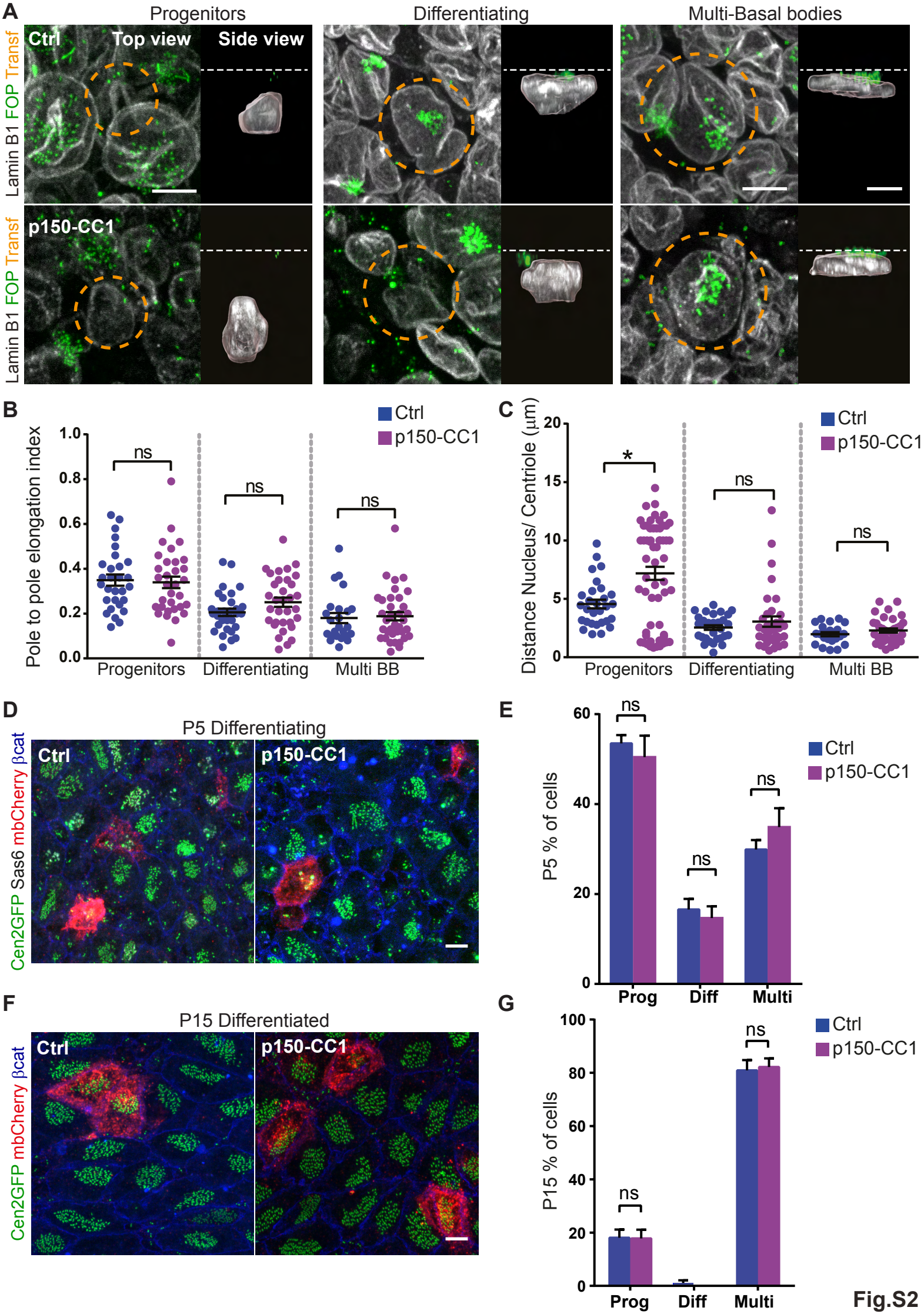
A
Progenitors
Differentiating
Multi-Basal bodies
Ctrl
Top view
Side view
p150-CC1
Lamin B1 FOP Transf
B
Ctrl
p150-CC1
Pole to pole elongation index
ns
Progenitors
Differentiating
Multi BB
C
Distance Nucleus/ Centriole (µm)
*
D
P5 Differentiating
Cen2GFP Sas6 mbCherry βcat
E
P5 % of cells
Prog
Diff
Multi
F
P15 Differentiated
G
P15 % of cells
Fig.S2

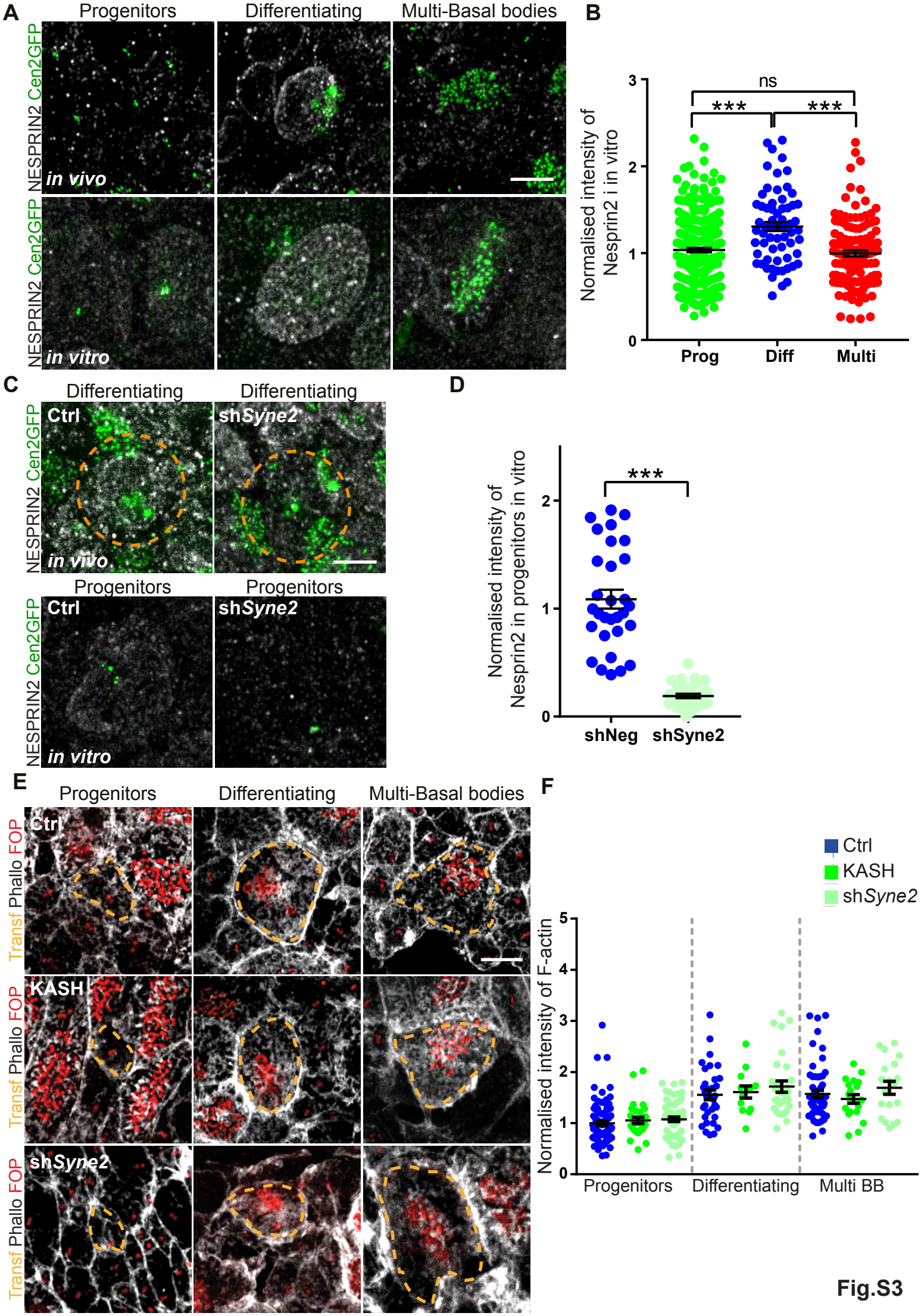
A
Progenitors
Differentiating
Multi-Basal bodies
NESPRIN2 Cen2GFP
in vivo
in vitro
B
Normalised intensity of Nesprin2 i in vitro
ns
***
***
Prog
Diff
Multi
C
Differentiating
Differentiating
Ctrl
shSyne2
Progenitors
Progenitors
D
Normalised intensity of Nesprin2 in progenitors in vitro
***
shNeg
shSyne2
E
Progenitors
Differentiating
Multi-Basal bodies
Transf Phallo FOP
Ctrl
KASH
shSyne2
F
Ctrl
KASH
shSyne2
Normalised intensity of F-actin
Progenitors
Differentiating
Multi BB

Fig.S3

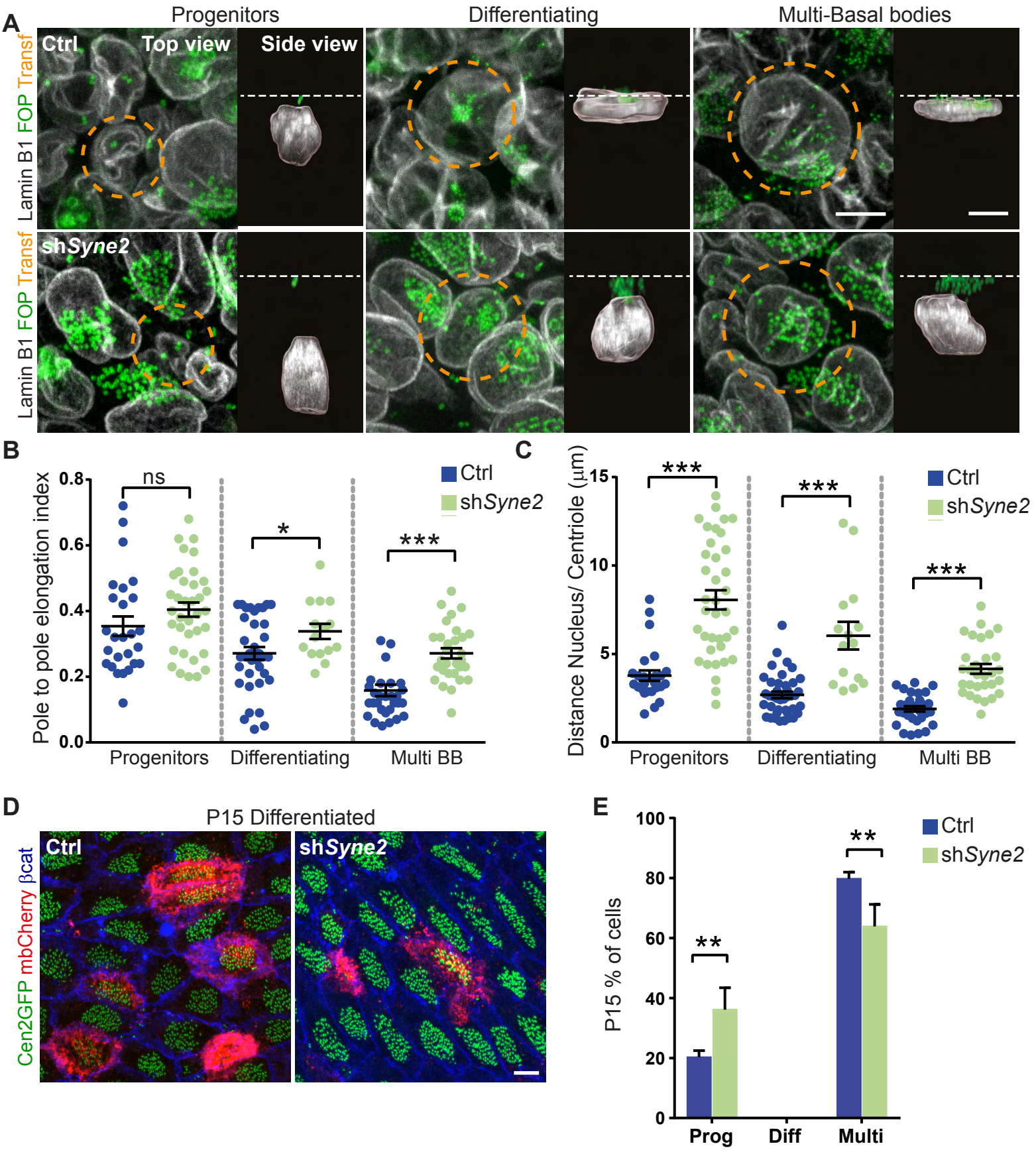
A
Progenitors
Differentiating
Multi-Basal bodies
Ctrl
Top view
Side view
shSyne2
Lamin B1 FOP Transf
B
Pole to pole elongation index
ns
*
***
Ctrl
shSyne2
Progenitors
Differentiating
Multi BB
C
Distance Nucleus/ Centriole (µm)
***
***
***
Ctrl
shSyne2
Progenitors
Differentiating
Multi BB
D
P15 Differentiated
Ctrl
shSyne2
Cen2GFP mbCherry βcat
E
P15 % of cells
**
**
Ctrl
shSyne2
Prog
Diff
Multi

Fig. S4

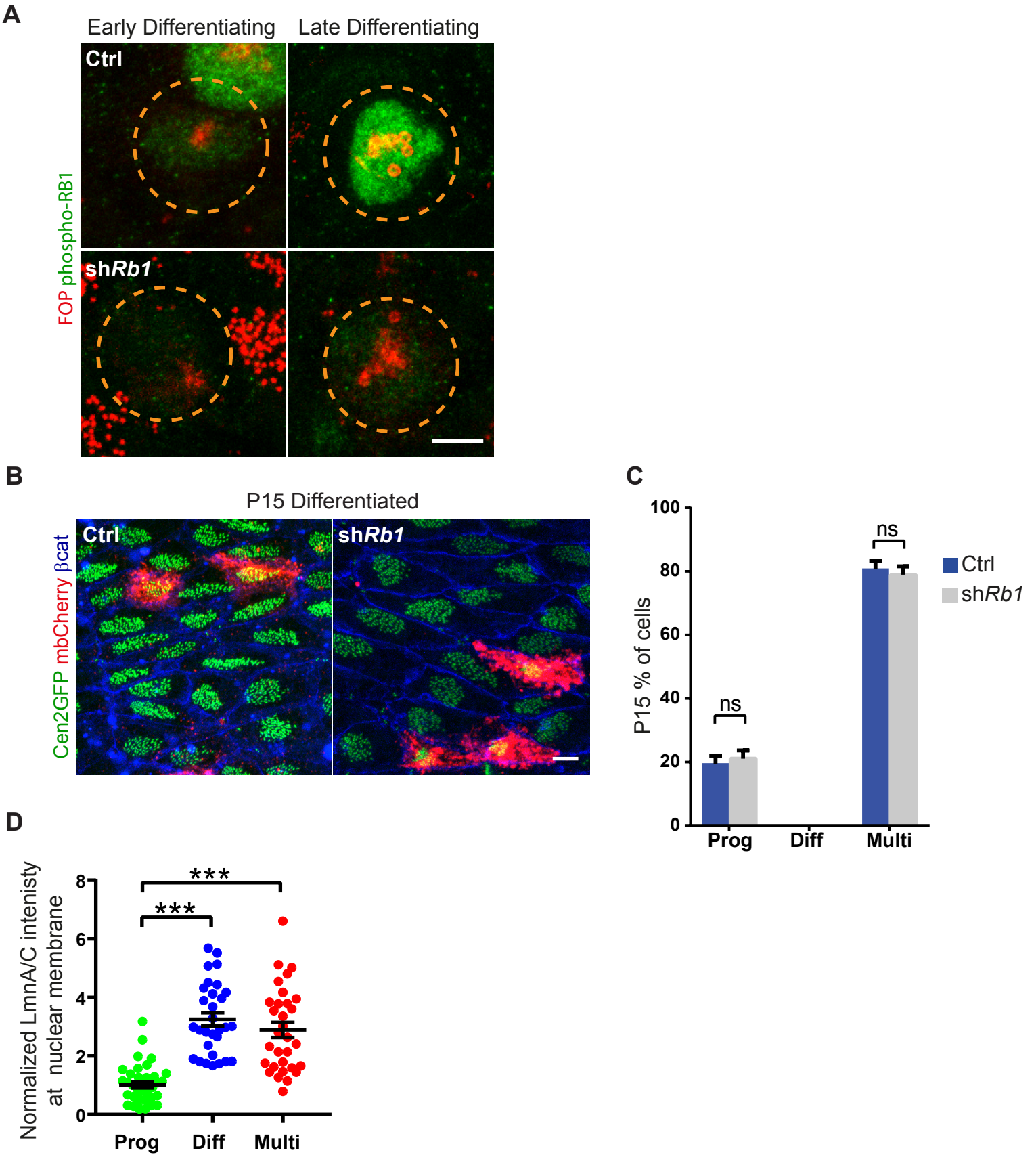
A
Early Differentiating
Late Differentiating
Ctrl
shRb1
FOP phospho-RB1
B
P15 Differentiated
Ctrl
shRb1
Cen2GFP mbCherry βcat
C
P15 % of cells
100
80
60
40
20
0
ns
ns
Ctrl
shRb1
Prog
Diff
Multi
D
Normalized LmnA/C intenisty at nuclear membrane
8
6
4
2
0
***
***
Prog
Diff
Multi

Fig. S5